The Astrophysical Journal Supplement Series, 258:32 (20pp), 2022 February https://doi.org/10.3847/1538-4365/ac3761

The Preprocessing of Galaxies in the Early Stages of Cluster Formation in Abell 1882 at $z = 0.139$

Aparajita Sengupta[1], William C. Keel[2], Glenn Morrison[3,4], Rogier A. Windhorst[5], Neal Miller[6], and Brent Smith[5]
[1] Department of Physics, Indiana University–Purdue University, Indianapolis, IN 46202, USA
[2] Department of Physics and Astronomy, University of Alabama, Tuscaloosa, AL 35487, USA
[3] Institute for Astronomy, University of Hawaii, Honolulu, HI, 96822, USA
[4] Canada-France-Hawaii Telescope, Kamuela, HI, 96743, USA
[5] School of Earth & Space Exploration, Arizona State University, Tempe, AZ 85287-1404, USA
[6] Department of Mathematics and Physics, Stevenson University, Owings Mills, MD 21117, USA
Received 2021 February 11; revised 2021 October 9; accepted 2021 October 25; published 2022 January 31

Abstract

A rare opportunity to distinguish between internal and environmental effects on galaxy evolution is afforded by "SuperGroups," systems that are rich and massive, but include several comparably rich substructures, surrounded by filaments. We present here a multiwavelength photometric and spectroscopic study of the galaxy population in the SuperGroup Abell 1882 (A1882) at $z = 0.139$, combining new data from the MMT and Hectospec with archival results from the Galaxy And Mass Assembly survey, the Sloan Digital Sky Survey, the Nasa/IPAC Extragalactic Database, the Gemini Multi-Object Spectrograph, and the Galaxy Evolution Explorer. These provide spectroscopic classifications for 526 member galaxies, across wide ranges of local density and velocity dispersion. We identify three prominent filaments along which galaxies seem to be entering the SuperGroup (mostly in E–W directions). A1882 has a well-populated red sequence, containing most galaxies with stellar mass $>10^{10.5}$ $M_{\rm Sun}$, and a pronounced color–density relation even within its substructures. Thus, galaxy evolution responds to the external environment as strongly in these unrelaxed systems as we find in rich and relaxed clusters. From these data, local density remains the primary factor, with a secondary role for distance from the inferred center of the entire structure's potential well. The effects on star formation, as traced by optical and near-UV colors, depend on galaxy mass. We see changes in lower-mass galaxies ($M < 10^{10.5}$ $M_{\rm Sun}$) at four times the virial radius of major substructures, while the more massive near-UV Green Valley galaxies show low levels of star formation within two virial radii. The suppression of star formation ("quenching") occurs in the infall regions of these structures even before the galaxies enter the denser group environment.

Unified Astronomy Thesaurus concepts: Abell clusters (9); Galaxy environments (2029); Starburst galaxies (1570); Galaxy evolution (594); Galaxy quenching (2040)

Supporting material: machine-readable tables

1. Introduction

The past three decades of observations and simulations have resulted in the paradigm of the ΛCDM hierarchical structure formation of the universe, in which clusters grow in size, mass, and richness by the accretion of isolated galaxies and galaxy groups along filaments (e.g., Huchra & Geller 1982; York et al. 2000; Colless et al. 2001; Springel et al. 2006).

Simulations show that a significant fraction (∼25%–40%) of galaxy accretion into halo masses ranging from $10^{12.9}$ to $10^{15.3}h^{-1}M_{\odot}$ between redshifts $z \sim 0$–1.5 occurs through groups, rather than individual galaxies (e.g., Berrier et al. 2009; McGee et al. 2009).

Strong empirical evidence connects galaxy environments to galaxy properties, such as color, star formation (SF) capabilities, morphologies, dynamics, etc. (e.g., Spitzer & Baade 1951; Smail et al. 1997; Dressler et al. 1999; Poggianti et al. 2006), and suggests that these properties vary significantly between galaxies in the "field" and in well-virialized clusters. The morphology–density relation of galaxies has proven to be remarkably robust both in clusters (up to redshift $z \simeq 1$) and in nearby groups (e.g., Dressler 1980; Postman & Geller 1984; Dressler et al. 1997; Postman et al. 2005; Treu et al. 2003; Smith et al. 2005). Higher-density regions harbor older red populations with significantly suppressed SF rates compared to the lower-density regions. The color–density relation appears at least as early as redshifts $z \sim 1.5$ (Cooper et al. 2007; Fassbender et al. 2011). The SF–density relation and related galaxy properties—e.g., color–density, average stellar age–density, and SF history–density—have been shown, at least at low redshifts, to exist not only within the cluster virial radius, but also in the cluster outskirts, as well as in groups and the field, indicating the preprocessing of galaxies before they enter the main cluster environment (e.g., Spitzer & Baade 1951; Hashimoto et al. 1998; Lewis et al. 2002; Pimbblet et al. 2002; Gómez et al. 2003; Fujita 2004; Balogh et al. 2004; Kauffmann et al. 2004; Baldry et al. 2006; Mahajan et al. 2010, 2011). In order to reconstruct galaxy transformation in the contexts of metallicity, color, morphology, SF history (SFH), active galactic nucleus activity, etc., one needs a panchromatic approach to study galaxy transformations as a function of environment, and to compare these data with the growing body of predictions from simulations.

Whether these transformations occur primarily as a result of a single dominant mechanism (e.g., ram pressure stripping due to the intracluster medium) or a combination of multiple

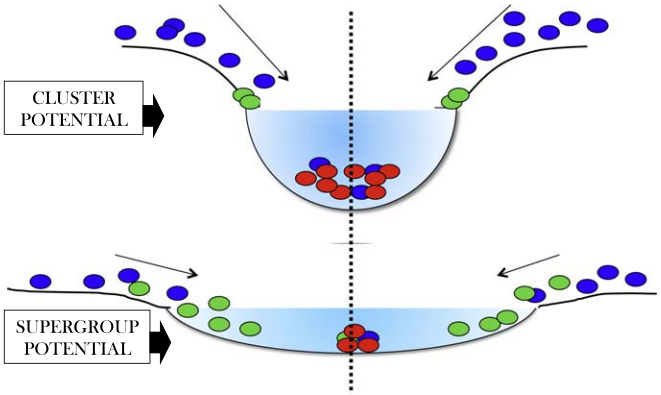

Figure 1. The schematic diagram shows galaxy evolution in a Cluster vs. a SuperGroup environment. A SuperGroup has a shallower but wider effective dark matter potential (bottom) compared to that of a Cluster (top). The blue and red circles represent star-forming and non-star-forming galaxies, respectively. The green circles represent the transition state ("Green Valley") galaxies between the two.

mechanisms acting over various spatial and temporal scales is not clear. In relaxed clusters, several evolutionary mechanisms act on similar spatial and temporal scales, making it almost impossible to disentangle the different local and global mechanisms, and ram pressure stripping appears to be the most dominant mechanism. An unrelaxed cluster or a cluster/filament precursor, on the other hand, has a shallower dark matter potential. Hence, the accreting galaxies are subjected to evolutionary mechanisms over larger spatial and temporal scales, unlike in more virialized clusters (Figure 1). This gives us a rare opportunity to study early galaxy transformations that are otherwise difficult to disentangle once cluster-centric mechanisms begin to dominate. With extensive spectroscopy and photometric imaging of the galaxies in the cluster outskirts, one can ideally map the radial locations of these transformations onto a time sequence. This will help to separate the processes that are otherwise superimposed in rich cluster–filament interfaces, and hence facilitate our understanding of the interactions between filaments and cluster cores at a different dynamical scale compared to a more evolved and relaxed system.

In this paper, we present a detailed photometric and spectroscopic map of the SuperGroup Complex of A1882.

The questions we address in this work are stated as follows. (i) At which point during the early evolutionary history of the formation of a cluster does one see significant galaxy transformations that lead to the overabundance of optically red galaxies that are observed at the core of the present-day clusters? In other words, are the well-established color–color and color–density relations seen in the present-day clusters also seen in an unrelaxed cluster like A1882? (ii) Is there evidence of galaxy transformation as a function of both the number density of the galaxies and the spatial locations of the galaxies within the structure? (iii) Is the galaxy transformation dependent on the mass of the galaxy?

This paper is organized as follows. In Section 1.1, we review the results of the previous work on the SuperGroup environment of A1882. In Section 2, we describe the observations and data selection. In Section 3, we quantify the complex environment of A1882. In Section 4, we present the results and their implications. And in Section 5, we present our main results.

The total current stellar masses and the k-corrections for this work have been obtained from the KCORRECT package `v3_2` (Blanton et al. 2003). The adopted cosmology for this work is $H_0 = 71$ km s^{-1} Mpc^{-1}, $\Omega_M = 0.27$, and $\Omega_\Lambda = 0.73$, as recommended by cosmic microwave background analysis (Planck Collaboration et al. 2020). All the positions are expressed in epoch J2000 coordinates.

1.1. The SuperGroup Complex A1882

Even with only a handful of unrelaxed clusters observed at low redshifts (Gómez et al. 2003; Brough et al. 2006; Tran et al. 2009; Einasto et al. 2020), it is clear that these are diverse in structure. Hence, there may be several pathways to a virialized cluster, a "SuperGroup" being one such pathway. A SuperGroup is a "group of groups" of galaxies that are in the process of coalescing, and that will eventually accrete enough mass to form a cluster.

The SuperGroup A1882 (Morrison et al. 2003; Erkurt et al. 2009; Owers et al. 2013) is associated with a highly diverse large-scale filamentary environment.

It has a redshift of $z = 0.139$, and is centered approximately at $\alpha = 14^{\rm h}14^{\rm m}39\overset{\rm s}{.}9$ and $\delta = -00°19'57''$ (J2000). It covers a much wider area than most of the previously observed intermediate-redshift relaxed clusters. A1882 consists of at least three virialized groups, which form the core of the structure, and the filamentary outskirts indicate that it is still accreting mass. Hence, the local galaxy density and projected structure-centric distances are sufficiently decoupled to trace the galaxy evolution mechanisms in the different environments within the system.

This provides a unique low-redshift opportunity to explore the formation process of a cluster of galaxies from its original group/filament precursors. By comparing the kinematical data with N-body numerical simulations, the mass of the system is estimated to be $M/M_\odot \sim 2 \times 10^{14}$, which means that the system will coalesce into a Coma-like cluster in $\sim$2 Gyr (Gomez et al. 2010; see also Gonzalez et al. 2005; Brough et al. 2006).

A combined optical and X-ray analysis by Owers et al. (2013) shows that two of the central galaxy groups appear to lie within a 1–1.5 $r_{\rm virial}$ (virial radius) of each other. This leads to a central dense region or the "swept-up" region—as defined by Vijayaraghavan & Ricker (2013)—between the three major groups, where the outer halos of the groups overlap. This "swept-up" region in A1882 has a higher galaxy number density than the outskirts, but is more tenuous than the groups themselves.

These factors strongly indicate that although A1882 contains dynamically mature groups, with their own individual well-formed X-ray structures, it is nonetheless a dynamically young system on a larger scale.

2. Observations and Data Reduction

We have constructed the largest available optical and UV galaxy catalog for the A1882 SuperGroup, containing 526 member galaxies based on their redshift distribution. This catalog contains the spectra of galaxies from the multiple galaxy groups that form the core of the SuperGroup, as well as the feeding filaments and the infall region. These contrasting environments provide us with an ideal laboratory for the study of galaxy evolution as driven by structure formation (Figure 5). We have complemented the optical spectroscopic data from the MMT and Hectospec at Mt. Hopkins with data from the Sloan Digital Sky

Table 1
Number of Galaxies Obtained from Different Surveys

Survey	No. of Galaxies with Spectroscopic Redshift	Radius of Sample (deg)	Radius of Sample (Mpc)	AB Limit (mag)
MMT/Hectospec	210	0.54	4.74	$r \leqslant 21$
Galaxy And Mass Assembly Survey	170	1.05	9.14	$r \leqslant 19.8$
Sloan Digital Sky Survey	85	0.74	6.41	$r \leqslant 17.8$
Gemini Multi-Object Spectrographs	38	0.17	1.5	$r \leqslant 22$
NASA/IPAC Extragalactic Database	23	0.68	6	⋯
GALEX (NUV)	192	0.57	4.97	⋯

Table 2
Galaxy Catalog of A1882 (Spectral Data)

Name	R.A. (J2000) (deg)	Decl. (J2000) (deg)	Redshift	Error (Redshift)	EW (Hα) (Å)	Error (EW(Hα)) (Å)	D_n4000
1	213.57009	−0.40192	0.138	1.51E-05	−11.81	1.66	1.38
2	213.50627	−0.22117	0.136	2.57E-05	−20.49	3.98	1.13
3	213.49960	−0.33654	0.136	3.16E-05	−11.81	0.88	1.87
4	213.58050	−0.44757	0.139	5.56E-05	−38.64	1.13	1.16
5	213.64855	−0.36581	0.140	2.08E-05	−21.21	0.59	1.18
6	213.56176	−0.42153	0.135	1.57E-05	−0.646	1.08	1.77
7	213.43641	−0.41416	0.139	6.94E-05	−26.34	2.66	1.31
8	213.65039	−0.33813	0.138	1.45E-05	−10.53	0.48	1.45
9	213.45533	−0.42338	0.138	2.09E-05	−4.292	1.76	1.47
10	213.53138	−0.39634	0.140	1.28E-05	−1.544	1.48	1.60

(This table is available in its entirety in machine-readable form.)

Survey (SDSS), the Galaxy And Mass Assembly (GAMA), the NASA/IPAC Extragalactic Database (NED), and the Galaxy Evolution Explorer (GALEX). We also have data from targeted observations using the Gemini Multi-Object Spectrograph (GMOS) on Gemini South (Gomez et al. 2010; Miller et al. 2010). We then matched the final optical galaxy catalog with the near-UV (NUV) data from the GALEX archive (GALEX program cycle: GI2-035; Principal Investigator: Neal Miller). Table 1 lists the number of galaxies obtained from the various surveys. Tables 2 and 3 list the spectrometric and photometric data, respectively, for the galaxies in A1882.

2.1. MMT/Hectospec

The Hectospec fiber system on the 6.5 m MMT (Fabricant et al. 2005, 2008) can place 300 fibers over a field of about 1°, or 8.7 Mpc at the mean redshift of A1882. This is large enough to include both the SuperGroup and the infall region, along with its feeding filaments. It samples a vast range of galaxy environments in a single MMT pointing. We targeted the galaxy population to $r \leqslant 21$ ($M_{\rm stellar} + 4$) and $\log(M_{\rm stellar}/M_{\odot}) \leqslant 8.23$. This enabled us to sample the faint magnitude, low-mass end of the galaxy mass spectrum out to a very large radius and deep into the feeding filaments, thus probing galaxy transformations in the far outskirts of the SuperGroup to very faint dwarf galaxies at this redshift. The selection priority for the MMT observations used 24 μm detections. Hence, the far-IR emitting galaxies in A1882 have a higher probability of having MMT spectra than other galaxies in our sample set. We employed 5 fiber configurations with 30 sky fibers, and 5 for spectrophotometric standards, leaving 265 target fibers per configuration. Given the possibility of probe collisions, a secondary target list was constructed in the same manner as the primary, but requiring weaker 24 μm emission ($\sim 5\sigma$). We used the 270 l mm^{-1} grating, yielding a spectral range of 3650–9200 Å. One hour of on-sky integration in three 20 minute exposures per configuration gave us signal-to-noise ratio (S/N) > 5 for all emission line galaxies. Most of the 24 μm sources have emission lines, making redshift estimates easier than using absorption spectral features.

Galaxy redshifts were measured using Fourier Cross-Correlation (FXCOR) and the SPLOT task in IRAF.[7] We applied FXCOR to the part of the spectrum shortward of the atmospheric oxygen line (5577 Å), which includes a sufficient

Table 3
Galaxy Catalog of A1882 (Photometric Data)

Name	$u-r$ (AB Mag)	Error ($u-r$) (AB Mag)	NUV−r (AB Mag)	Error (NUV−r) (AB Mag)	Log (Mass)	Source
1	1.65	0.01	2.74	0.08	9.83	MMT
2	4.39	0.09	1.50	0.14	9.31	MMT
3	2.80	0.02	⋯	⋯	9.74	MMT
4	2.63	0.02	⋯	⋯	10.03	MMT
5	1.57	0.05	⋯	⋯	9.02	MMT
6	1.89	0.02	3.41	0.18	9.64	MMT
7	2.56	0.10	0.72	0.16	8.97	MMT
8	2.22	0.01	4.18	0.13	10.20	MMT
9	2.17	0.01	4.15	0.23	9.85	MMT
10	2.67	0.00	5.18	0.11	10.78	MMT

(This table is available in its entirety in machine-readable form.)

[7] IRAF is distributed by the National Optical Astronomy Observatories, which are operated by the Association of Universities for Research in Astronomy, Inc., under cooperative agreement with the National Science Foundation.

number of well-defined emission and absorption lines to provide an accurate galaxy redshift. The template spectra came from the Kennicutt atlas (Kennicutt 2004). Using the SPLOT task, we measured the wavelengths of the significant absorption and emission lines—H_α, H_β, [N II], Ca II K and H, [O II], and [O III]—to manually determine the redshift of each individual galaxy. We then compared these redshifts with those obtained from the MMT pipeline. The redshift values obtained for the galaxies by employing these different techniques are largely consistent.

2.2. The Data from the Galaxy And Mass Assembly Survey

The GAMA survey (Liske & Baldry 2015) builds on existing widefield spectroscopic surveys like SDSS, the 2dF Galaxy Redshift Survey, and the Millennium Galaxy Catalogue, down to r magnitude <19.8 mag and $M^\star$+2 mag at $z \sim 0.139$, where $M^\star$ is the characteristic absolute magnitude in the Schechter function. The GAMA fiber diameter is 2.0" or 5.9 kpc at this redshift.

The emission and absorption lines were measured with SPLOT in batch mode after the lines were fitted using Gaussian profiles. The continuum for each line was selected using the recommendation in the SDSS archive. Only those lines that are within ±10 Å of the recommended line centers are used for detections in the redshift fitting. Several spectra from the GAMA survey have a low S/N in the bluer wavelength regime, hence the detections of Hδ at 4100 Å and ([O II]) at 3726 Å are not reliable for those spectra, and have been discarded. Manual measurements were made for equivalent width (EW) values that were obtained incorrectly by the IRAF script, due to a discontinuity in the continuum of the spectra and/or a low S/N.

The spectra for the GAMA survey have been flux scaled, centered at 6300 Å (6200–6400 Å) to match those of the MMT, for consistency.

2.3. The Sloan Digital Sky Survey

We used archival data from Data Release 12 (Alam & Albareti 2015). We retrieved galaxy data centered at $\alpha = 14^{\rm h}14^{\rm m}39\overset{\rm s}{.}9$ and $\delta = -00°19'57''$ (J2000), within a radius of 45′ and with a redshift range of $0.133 < z < 0.144$.

The SDSS spectroscopic sample is incomplete for galaxies with nearby neighbors. This is due to the fact that the fibers cannot be very close together, typically less than 55″. Corrections for these missing objects are needed for the statistical correction of the spectroscopic catalogs.

2.4. The Galaxy Evolution Explorer Data

SDSS only samples data within 3″-diameter regions at the center of each galaxy. However, GALEX samples the entire galaxy. The NUV data were obtained from the GALEX archive (Martin et al. 2005; Morrissey et al. 2007), and selected within a 5″ radius of each optical galaxy. K-corrections were applied, and Galactic foreground extinction in the UV was applied using the recipe from Cardelli et al. (1989), using $A_{\rm BV} = \left(a(\lambda) + \frac{b(\lambda)}{R_v}\right) \times E(B-V)$, where R_v parameterizes the extinction law and λ is the wavelength. For most locations in the Milky Way, $R_v = 3.1$ is a representative value and the Galactic extinction is E(B–V) = 0.041 mag toward A1882. We scaled to $\lambda = 2800$ Å in the NUV, and found the Galactic extinction for the NUV to be about 0.08 mag. We chose the NUV for our analysis because ∼36% of the NUV data matches our optical catalog, whereas only ∼24% of the FUV data matches our optical catalog. In addition, the NUV–r color correlates more strongly with the specific star formation rate of galaxies than the FUV − r color (e.g., Salim 2014).

A reference cluster center position was determined by eye at roughly equal distances from the three major optical groups. The member galaxies are constrained within a redshift range of $0.133 \leqslant z \leqslant 0.144$ and a radius of $1\overset{\circ}{.}05$ or 9.14 Mpc from the adopted center of A1882 at $\alpha = 14^{\rm h}14^{\rm m}39\overset{\rm s}{.}9$ and $\delta = -00°19'57''$ (J2000), as shown in Figure 2(a). The red histogram represents all 1185 of the galaxy spectra obtained using the MMT and Hectospec that have been used to constrain the catalog. The blue histogram shows all of the additional member galaxies obtained from GAMA, the SDSS archive, NED, and GMOS. The dashed vertical lines mark the adopted redshift cutoffs for A1882 ($0.133 < z < 0.144$). The galaxy groups are defined as circles with diameters of ∼1 Mpc each, with their centers in epoch J2000 coordinates at ($\alpha = 14^{\rm h}15^{\rm m}07^{\rm s}$, $\delta = -00°29'35''$), ($\alpha = 14^{\rm h}14^{\rm m}24^{\rm s}$, $\delta = -00°22'46''$), and ($\alpha = 14^{\rm h}14.07^{\rm m}15^{\rm s}$, $\delta = -00°21'00''$), respectively. The centers of the first two galaxy groups were adopted from Owers et al. (2013), whereas the third group was determined from the spatial distribution of optical galaxies in our catalog. A circle with a diameter of ∼3 Mpc encloses the three groups and the "swept-up" region. As expected in a virializing system, the infall and orbiting of the galaxies together produce near trumpet-shaped line-of-sight velocity profiles in the cluster region, as shown in Figure 2(b). A1882 does not have a single central concentration, much less an obvious brightest cluster galaxy. Hence, we use the formula $c\Delta z/(1+z_{\rm mean})$ for the line-of-sight velocity to correct for the nonlinear mapping of the redshift to the velocity. The entire SuperGroup A1882, with its groups and feeding filaments, has a velocity dispersion of 620 km s^{-1}. This value is lower than the values for more massive and relaxed clusters, such as the Coma cluster, which have $\sigma \simeq 1000$ km s^{-1} (e.g., Rood 1970). The velocity dispersions of Group 1, Group 2, and Group 3, from their respective centers (not from the assumed center of Abell1881), are ∼669 km s^{-1}, ∼687 km s^{-1}, and ∼621 km s^{-1}, respectively (as shown in red, blue, and green, respectively, in Figure 2(b)). The orange crosses represent the line-of-sight velocities for the "swept-up" region. The blue dashed line shows a linear model fit with 95% confidence interval (CI). The velocity dispersions of the galaxies in the filaments range from ∼490 km s^{-1} for Filament 3 to ∼769 km s^{-1} for Filament 2, and the velocity dispersion for Filament 1 is ∼550 km s^{-1}. The velocity dispersion for the galaxies that are further away from the assumed center of the SuperGroup, and not members of the galaxy groups, filaments, or the "swept-up" region, is ∼543 km s^{-1}. The velocity dispersions for the galaxy groups are much higher than the velocity dispersion for the galaxies in the lower-density outskirts, as expected. That is, the groups are significantly on the way to virialization, if they are not already there.

3. Quantifying the Galaxy Environment within A1882

3.1. Local Galaxy Density (Σ) Profile of A1882

We have calculated the projected local galaxy density (Σ) in Mpc^{-2} for each of the N galaxies using the nth nearest neighbor

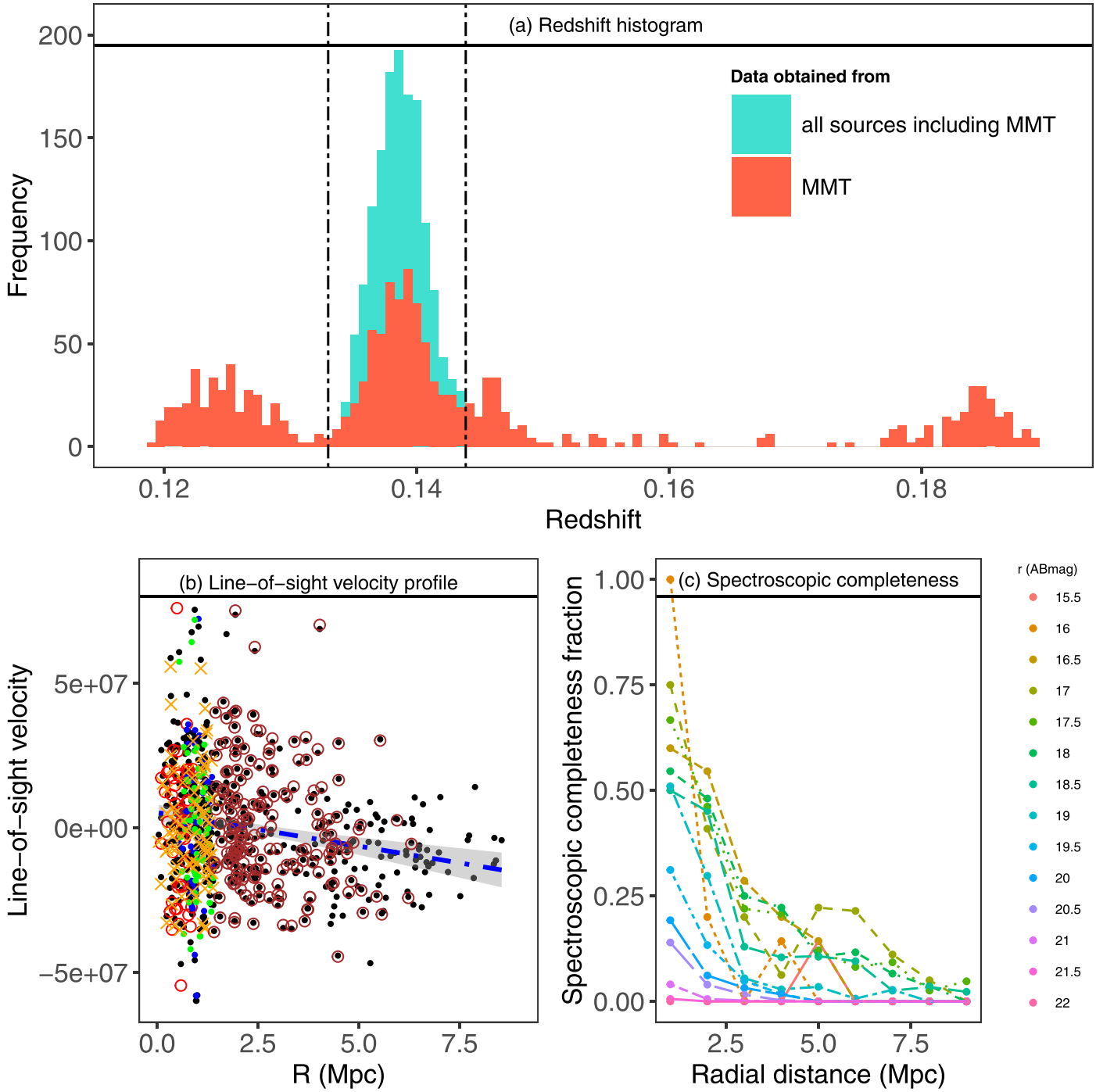

Figure 2. (a) Redshift histogram of SuperGroup A1882. (b) Line-of-sight velocity profiles of the A1882 galaxies. The red, blue, and green circles represent the line-of-sight velocities for the galaxies in Group 1, Group 2, and Group 3, from their respective centers. The orange crosses represent the line-of-sight velocities for the "swept-up" region. The brown open circles are the velocities of the filaments of galaxies. The blue dashed line shows a linear model fit with 95% CI. (c) Spectroscopic completeness for A1882 as a function of r-magnitude and the cluster-centric radius in megaparsecs.

algorithm. In order to obtain a robust estimation of Σ, we follow Baldry et al. (2006), where Σ_N is given by $\frac{N}{\pi d_N^2}$ and d_N is the averaged projected comoving distance of a galaxy from its fourth- and fifth-nearest neighbors.

Figure 3(a) shows the trend of the projected local galaxy density Σ with projected cluster-centric radius R, using locally weighted scatterplot smoothing. The three major galaxy groups are shown in red, the galaxies in the "swept-up" region are shown in green, and the galaxies within the feeding filaments are shown in blue. The galaxies indicated in black are member galaxies of A1882 that do not lie within any of the galaxy groups, filaments, or the "swept-up" region. We will refer to these galaxies as "others." The yellow line represents the running mean of Σ at various projected radial distances.

In order to quantify the correlation between the local galaxy density (Σ) and the projected cluster-centric radius R, we first compute the p-value ($<2.2 \times 10^{-16}$). This value is less than 0.05 or 5%. Hence, this correlation is rather significant. We

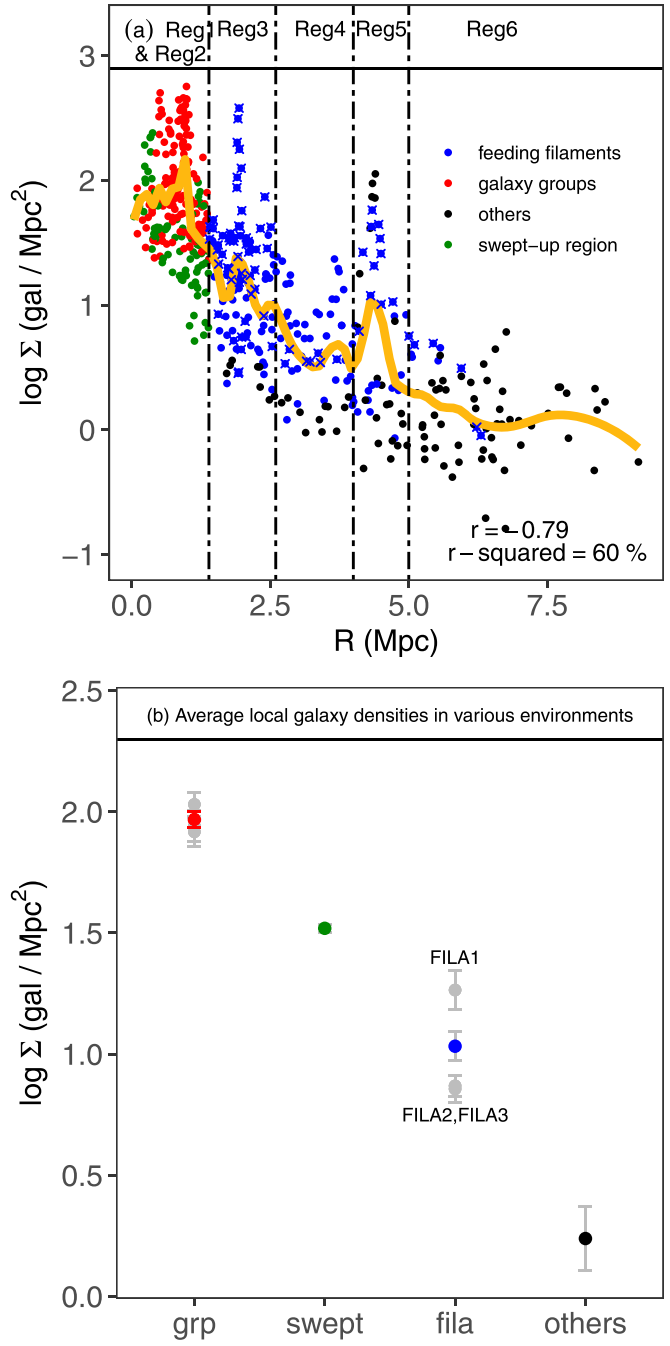

Figure 3. (a) Correlation plot of the projected radial distance $\mathcal{R}$ from the adopted center of A1882, and the local galaxy density Σ of the galaxies. The yellow line represents the running mean of Σ. (b) Average densities of galaxies in the three groups, the "swept-up" region, the feeding filaments, and the "others" (see Section 3.1 and Table 4), respectively, with standard error (1σ) bars. The average densities of the galaxies within the three individual filaments are shown in gray.

have further used the following guidelines for the magnitude of Pearson's product-moment correlation coefficient r, as defined in Evans (1996), where r measures the strength of a linear correlation between two variables and its statistical significance, as follows:

1. Positive and negative values of r signify positive and negative correlations, respectively;
2. 0.00–0.19 signifies "*very weak*" correlation;
3. 0.20–0.39 signifies "*weak*" correlation;
4. 0.40–0.59 signifies "*moderate*" correlation;
5. 0.60–0.79 signifies "*strong*" correlation; and
6. 0.80–1.00 signifies "*very strong*" correlation.

The correlation coefficient r is -0.79, thus signifying a "*strong*" negative correlation between $\log(\Sigma)$ and R.

3.2. Identifying Feeding Filaments Using the Friends-Of-Friends Algorithm

We have used the group searching code `groups_pro.c` (Ivan Valtchanov, 1998), based on the Friends-Of-Friends (FOF) percolation algorithm developed by Huchra & Geller (1982), to identify the feeding filaments in the cluster outskirts (Figure 4). This method recursively links all of the galaxies satisfying the linkage, based on the distances between the galaxies and their velocities. It then finds galaxy number density enhancements for galaxies with spectroscopic redshifts, thus identifying the galaxies that form the filaments. We define a filament as a structure containing at least three galaxies connected by the linkage parameters. We have detected three feeding filaments that are shown in red circles, aquamarine triangles, and yellow squares, and indicated by the blue arrows in Figure 4. See also Table 4 for more details. Figure 5 shows the optical galaxies (gray dots) in our catalog, overlaid with the galaxies detected in the NUV (blue dots) and the galaxies with H_α data (in red). Most of the NUV galaxies in the catalog lie within the groups, or in their immediate infall regions.

Tying this result back to Section 3.1, Figure 3(b) shows the mean Σ within each of the three groups, the "swept-up" region, the feeding filaments, and the "others." As expected, the groups have the highest local galaxy densities, and they have comparable values. The "swept-up" region exhibits a lower Σ than the groups, but is higher than the average Σ within the filaments. The galaxies that lie outside these structures, i.e., the "others," have the lowest Σ, as expected.

As mentioned in Section 3.1, we observe several overdensities as we move outward from the central galaxy groups. Most of these overdensities lie along Filament 1. This is clear from Figure 3(b), in which the average local galaxy densities of the individual filaments are shown in gray. The average Σ of Filament 1 is significantly higher than those of the other two filaments, as can also be seen in Figure 3(a) (blue crosses). The density contour (in gray) in Figure 4 points toward the possibility of an as yet undetected smaller galaxy group, or a galaxy group that is in the early stages of assembly within Filament 1, further to the right of the central galaxy groups.

Figure 6 presents a sideways view of SuperGroup A1882 with redshift. It can clearly be seen that the galaxies are being accreted asymmetrically, mostly along the direction of the R.A., which agrees well with the position of the majority of the detected feeding filaments.

3.3. Total Current Stellar Masses

The total current stellar masses have been obtained from the Bell and de Jong stellar mass model (Bell & de Jong 2001), using the IRAF KCORRECT package, which uses the SDSS absolute magnitudes. Photometric zero-point corrections, Galactic extinction corrections, and k-corrections have been applied to the observed magnitudes. We have divided the galaxies into three mass bins: *high-mass* galaxies ($M \geqslant 10^{10.5} M_\odot$); *intermediate-mass* galaxies ($10^{9.5} M_\odot \leqslant M \leqslant 10^{10.5} M_\odot$); and *dwarf galaxies* ($M < 10^{9.5} M_\odot$). The motivation for these mass divisions

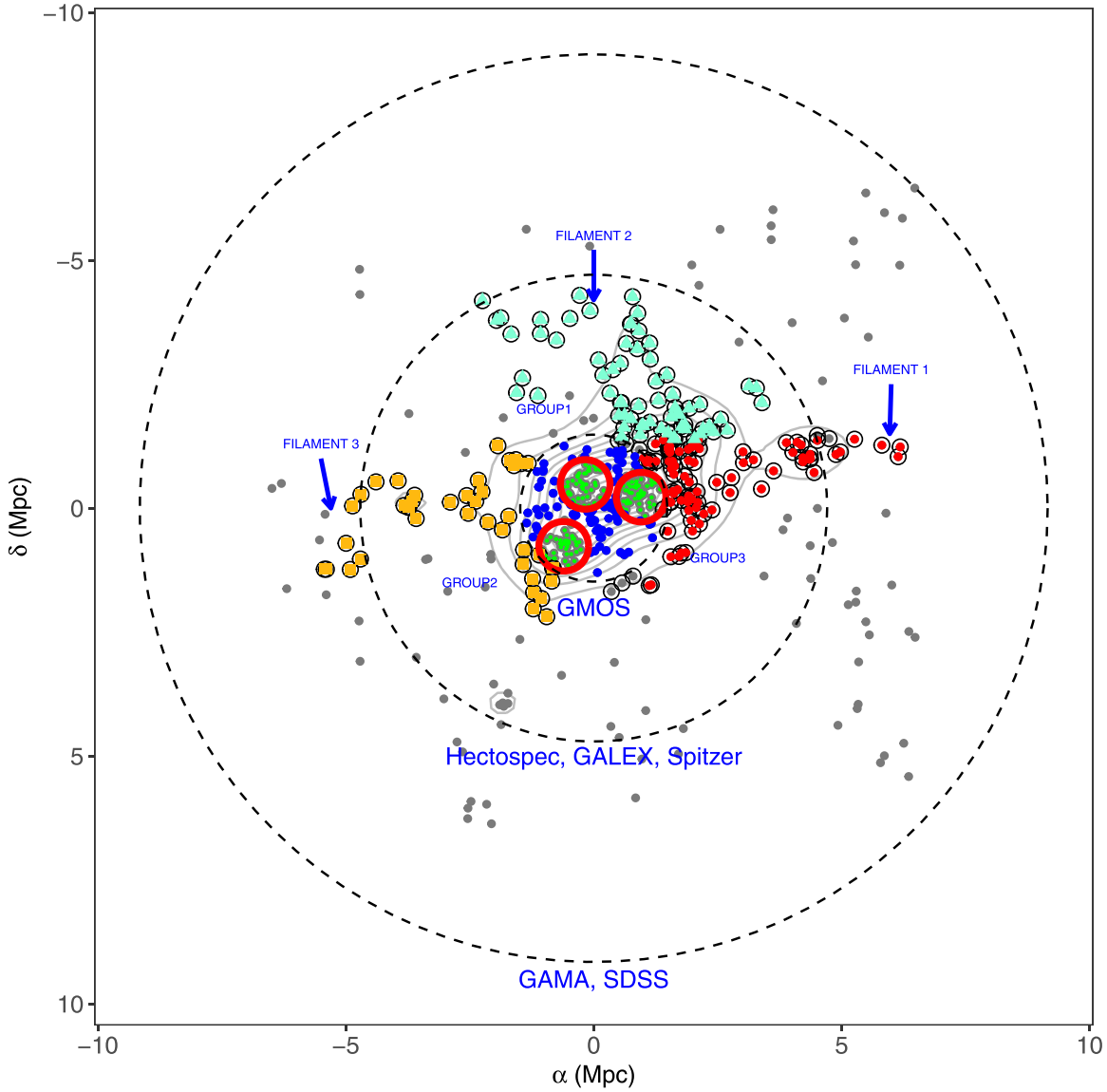

Figure 4. The three major filaments detected by the Friends-Of-Friends algorithm are shown in red dots, aquamarine triangles, and yellow squares, and also indicated by the blue arrows. The green dots encircled in red represent the galaxy group members. The blue dots represent the "swept-up" region. The gray dots represent all of the galaxies categorized as "others." The contours show a galaxy number density map. The dotted circles represent the areas covered by the various surveys used in the current work.

is that several studies have drawn attention to galaxies in the mass range of $M < 10^{9.5} M_{\odot}$, which show especially strong environmental transformations. The dwarf galaxies have been defined by the recipe provided by Blanton et al. (2001), or $z_{\rm AB} \geqslant 15$ mag and $M_z > M^* + 2.3$ mag for the Coma SuperCluster, where $M_z^* = -22.32$ mag. Using the above recipe, we get $z_{\rm AB} > 19.1$ mag for the dwarf galaxies at $z = 0.139$. The low-mass galaxies correspond reasonably well with this z-mag limit defined for dwarf galaxies in the Coma SuperCluster.

The MMT sampling goes fainter than the SDSS and GAMA survey limits, but covers only 1° in the sky. We have sampled further out, to ∼2° in the sky, using the SDSS and GAMA surveys. Hence, the dwarf galaxy sampling is sparser in the outskirts.

We further divide the galaxy environments into three different regions, as indicated in Figure 3(a) by the black vertical dotted–dashed lines. The regions are defined in 4.1.

4. The Color Evolution and Spatial Distribution of the Galaxies

4.1. Defining the Different Environments for a Comparison of Galaxy Evolution Indicators

Our catalog for A1882 covers a vast range within its density and velocity fields, from the dense central core to the sparse distant outskirts from where the galaxies pour into the central potential of the SuperGroup along the filaments. This scenario provides us with four distinct galaxy environments, as discussed in the previous sections, and as shown in Figure 4: (i) the group environments; (ii) the central dense region, or the "swept-up" region between the three major groups, where the outer gaseous halos of the groups overlap; (iii) the feeding filaments, as inferred from the FOF percolation algorithm; and (iv) the infalling galaxies that are not within the filament environment (categorized as "others").

Table 4
Numbers of Galaxies, Local Galaxy Densities, and Velocity Dispersions for Each Substructure within A1882

Structure Description	No. of Galaxies (in Optical)	No. of Galaxies (in NUV)	Σ (Mpc^{-2})	Velocity Dispersion (km s^{-1})
All environments in A1882	526	191	55	620
All galaxy groups	150	58	133	664
Group 1	49	⋯	112	669
Group 2	43	⋯	134	687
Group 3	58	⋯	150	621
"Swept-up" region	84	42	48	588
All three filaments	194	78	22	634
Filament 1	80	⋯	38	551
Filament 2	66	⋯	11	769
Filament 3	41	⋯	10	490
"Others"	97	13	6	543

From Table 4, Σ in the galaxy population categorized as "others" is the lowest within the environment of A1882, with a density of about 6 galaxies Mpc^{-2}. This population also exhibits a much lower velocity dispersion compared to the galaxy groups. The average Σ in the three filaments and the "swept-up" region are 22 galaxies Mpc^{-2} and 48 galaxies Mpc^{-2}, respectively. The galaxy groups have the highest Σ, as expected (133 galaxies Mpc^{-2}). Filament 1, which shows evidence of overdense regions in the far outskirts, has a much higher Σ compared to the other filaments. This filament is connected to Group 3, which also exhibits the highest Σ of all of the three galaxy groups. This reinforces the conclusion that the accretion of the galaxies into A1882 is highly asymmetric. Filament 1 also shows a much higher velocity dispersion compared to the other filaments, and also the galaxy groups, indicating an as yet undetected smaller galaxy group, or a galaxy group that is in the early stages of assembly, as mentioned in the previous section.

However, we observe distinct overdensities at various R values all the way out to about 7 Mpc, indicating that this SuperGroup is highly clumpy, which strongly suggests that it is still in the process of growing and accreting today. This clumpiness could potentially help in disentangling the roles of Σ and the radial positions of the galaxies in this SuperGroup environment. Hence, in addition to comparing the galaxy properties in the structures mentioned above, we will also trace the galaxy properties as a function of the radial distance from the assumed center of A1882, as shown with the black dashed vertical lines in Figure 3(a) (also see Table 5). This classification of the regions has been carefully chosen, in order to study the effects of the projected radial distances of the galaxies on their properties, as well as the effects of Σ and the underlying large-scale structures. Note that the galaxies in the filaments have been sampled in such a manner that they capture the overdensities in the filaments at various radial distances from the assumed center.

1. Region 1 and Region 2 coincide with the groups and the "swept-up" region, respectively, both of which lie within a radius of 1.4 Mpc from the assumed center of the SuperGroup.
2. Regions 3–6 contain galaxies within filaments as well as galaxies that are outside them ("others").
3. Region 3 lies between the radii of 1.4–2.6 Mpc. This region mostly consists of galaxies within filaments, as shown in blue in Figure 3(a). There is a distinct overdensity of galaxies in this region.
4. Region 4 lies between the radii of 2.6–4 Mpc. This region has a significantly lower Σ than Region 3, as shown in Figure 7.
5. Region 5 lies between the radii of 4–5 Mpc. This region shows an overdensity of filaments at this radial distance from the assumed center of A1882, and it has a higher Σ than Region 4.
6. Region 6 lies beyond a radius of 5 Mpc, and it has the lowest Σ. It is dominated by the galaxies categorized as "others."

We will examine various parameters, like u–r, NUV–r colors, and EW[$H\alpha$], with the various galaxy environments described in this section. We will then narrow down the possible locations for the quenching of galaxies that leads to the bimodality of colors that we see in the A1882 SuperGroup. In the following sections, the NUV–r color evolution inferences for the red galaxies are drawn only from the NUV bright galaxies, because of the incompleteness of the sample at the fainter magnitudes. Our sample in the NUV is restricted to within a radius of 4.7 Mpc from the adopted center. Hence, the NUV faint galaxies and/or very far outskirts are poorly represented.

4.2. Optical, UV Color–Magnitude, and Color–Mass Relations in A1882

In Figure 8(a), the best fits for Red Sequence (RS) galaxies (red lines) and Blue Cloud (BC) galaxies (blue lines) have been plotted in the u–r using the prescriptions from Baldry et al. (2004) and Balogh et al. (2004).

The color–magnitude diagram of the NUV galaxies (Figure 8(b)) has been plotted using the prescriptions from Wyder et al. (2007) and Baldry et al. (2004).

The flux-to-mass transformation is increasingly affected by the details of the exact SFH, as we consider shorter SF timescales. The NUV arises from the photospheres of O through late-type B-stars and early-type A-stars with mass $M \leqslant 3M_{\odot}$. Hence, the NUV measures the SF averaged over the lifetimes of these stars, i.e., the past gigayear (Kaviraj & Schawinski et al. 2007). This makes the NUV far more sensitive to recent and ongoing SF compared to the optical colors of the galaxies, which trace SF over a period of ∼2–3 Gyr. The H_{α} emitters are O-stars and early-type B-stars, with masses in excess of $17M_{\odot}$. These stars have lifetimes of a few million years. Hence, the H_{α}-emitting galaxies have undergone more recent significant SF episodes in the past 10^7 yr. H_{α} is only sensitive to high-level continuous SF. By contrast, the galaxies showing NUV emission, but no H_{α} emission, have recent, low-level SF.

We have reclassified the red, blue, and green galaxies, based on their optical and UV colors, as well as their EW[H_{α}]. In this paper, negative EW[H_{α}] represents H_{α}-emitting galaxies or the emission line galaxies. The red and green galaxies in optical and UV colors, with EW[H_{α}] < -2 Å, are possibly dusty

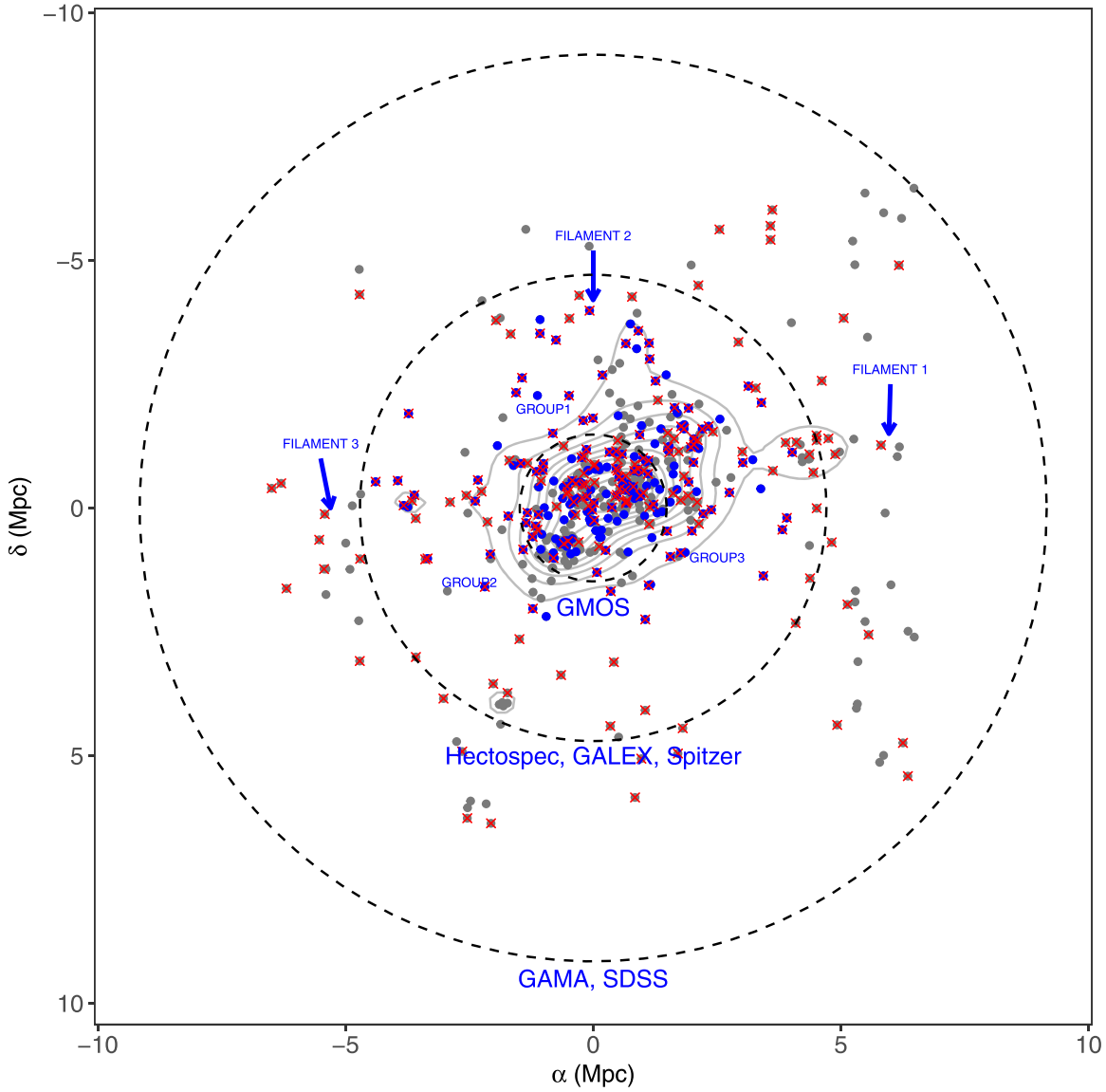

Figure 5. The optical galaxies overlaid with the galaxies detected in the NUV (blue dots) and the galaxies with H_α data (red crosses). The contours show a galaxy number density map.

starburst galaxies, and hence they have been reclassified as blue galaxies, in both the optical and UV colors. We have used this new classification for all of the figures in this paper, except the color–magnitude diagrams (Figure 8(a)–(b)).

A1882 has a well-defined optical RS, Green Valley (GV), and BC galaxies (Figure 8(a)). Although most of the galaxies fall within the 95% PI for all of the galaxies in the A1882 catalog (the black dashed lines), we see some RS galaxies that lie outside the PI, especially toward the reddest region of the *u*–*r* color, all of which are low- to intermediate-mass galaxies with $\log M/M_\odot < 10.5$ (Figure 10(a)). Some of these red galaxies are also H_α emitters, and have been reclassified as blue galaxies (shown with black circles in Figure 10(a)), thus signifying dusty starburst galaxies that have undergone recent SF in the past few million years. About 90% of the galaxies in the red *u*–*r* histogram in Figure 9(a) have mass $\log M/M_\odot > 10.5$.

A1882 also exhibits a clear bimodality in the NUV optical color–magnitude diagram, as shown in Figure 8(b).

We classify the galaxies in A1882 into the three following sequences, based on the NUV–*r* color–magnitude diagram:

1. Passive or RS galaxies (the red filled circles): the low-luminosity galaxies in the NUV, especially those on the RS, are significantly undercounted due to the GALEX flux detection threshold. Hence, by selection, all of the red galaxies on the RS represent only the massive NUV bright galaxies ($log\ M/M_\odot > 10.4$). In this sequence, only 7.5% of the galaxies are H_α emitters, i.e., most of these galaxies have no recent star-forming episodes in past 1 Gyr. The recent star-forming galaxies have been reclassified as star-forming sequence or BC (the blue filled circles). In addition, we have included optically red, *non*-H_α-emitting galaxies in the catalog of red NUV galaxies. We have selected these galaxies to match the coverage area of GALEX in A1882. Henceforth, RS or red galaxies will indicate only the *u*–*r* or NUV–*r* red galaxies that are not H_α emitters.

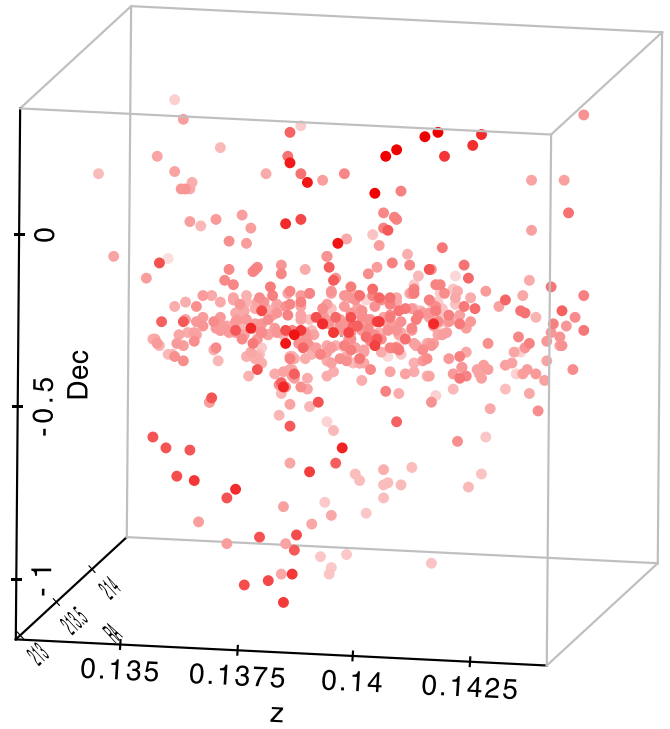

Figure 6. A redshift-decl. slice of SuperGroup A1882 with redshift. The dimmer red circles represent galaxies that are further away from that vantage point (i.e., the fainter the dots, the larger the value of their R.A.).

Table 5
Numbers of Galaxies, Local Galaxy Densities, and Velocity Dispersions for each Region within A1882, as Defined in Section 4.1

Region	Radial Distance (in Mpc)	Number of Galaxies Detected in Optical	Number of Galaxies Detected in NUV	Local Galaxy Density (Σ) (Galaxies Mpc^{-2})
Region 1	$\mathcal{R} < 1.4$	150	58	∼133
Region 2	$\mathcal{R} < 1.4$	84	42	∼48
Region 3	$1.4 < \mathcal{R} < 2.6$	121	53	∼29
Region 4	$2.6 < \mathcal{R} < 4$	58	34	∼7
Region 5	$4 < \mathcal{R} < 5$	47	4	∼17
Region 6	$\mathcal{R} > 5$	65	⋯	∼2

2. Star-forming sequence or BC (the blue filled circles): these galaxies are mostly blue in their NUV–r color, indicating star-forming episodes in at least the past 1 Gyr. About 67% of the galaxies in this sequence are H_α emitters, and hence have undergone recent significant SF in the past 10^7 years. Henceforth, BC or blue galaxies will indicate only the u–r or NUV–r blue galaxies, in addition to the H_α-emitting galaxies that were photometrically categorized as red or green.
3. The intermediate phase or GV galaxies (the green filled circles): this phase represents a transitional phase between the passive sequence and the star-forming sequence (see Kaviraj et al. 2005; Martin et al. 2007; Salim et al. 2007; Wyder et al. 2007; Schawinski et al. 2014). These galaxies have undergone recent low-level SF. However, a number of the GV galaxies in the NUV–r color show H_α emission (the black open circles in Figure 8(b)). These galaxies are possibly dusty starburst galaxies, indicating only recent ongoing starburst episodes (in the past few million years), and are hence undetected in the NUV color. These recent star-forming galaxies have been reclassified as star-forming sequence or BC (the blue filled circles). Henceforth, GV or green galaxies will indicate only the u–r or NUV–r green galaxies that are not H_α emitters.

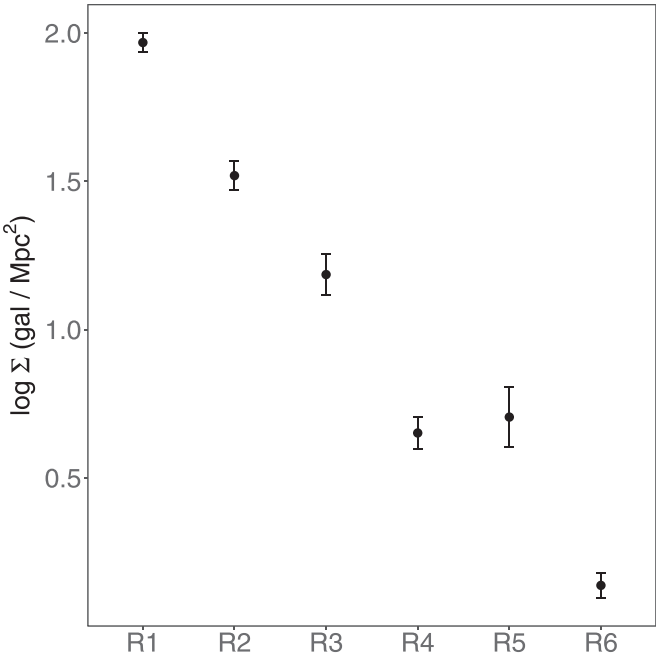

Figure 7. (a) Correlation plot of the regions (defined in Section 4.1 and Table 5) and Σ in A1882.

There are several pathways for galaxies to transition through the GV: (a) the galaxies could be transitioning from the BC to the RS as they are quenched; (b) minor, gas-rich mergers in passive galaxies (Kaviraj et al. 2005); and (c) RS galaxies may accrete gas from the intergalactic medium and undergo low-level SF (Thilker et al. 2007).

Figures 10(c)–(d) show the fractional numbers of the optical and NUV galaxies for the three different mass ranges. The high-mass, intermediate-mass, and dwarf galaxies are defined in Section 3.3. The RS, BC, and GV galaxies, as described above, are represented by red, blue, and green filled circles, respectively.

In both the optical and UV color, the high-mass population ($\log M/M_\odot > 10.5$) is dominated by the RS galaxies (∼63% and ∼74%, respectively). However, in stark contrast to the optical colors, the NUV color reveals a large number of GV galaxies (41 non-$H\alpha$-emitting GV galaxies in the NUV, compared to only 18 in optical color), most of which have $\log M/M_\odot > 9.5$. These are low-level recent star-forming galaxies in the past gigayear. This leads to significantly more pronounced GV galaxies in NUV–r color, despite the undercounting of the faintest galaxies due to the GALEX magnitude limit. Hence, the NUV is more effective in detecting low-level SF compared to its optical counterpart, and has revealed a significant number of low-level star-forming galaxies. These

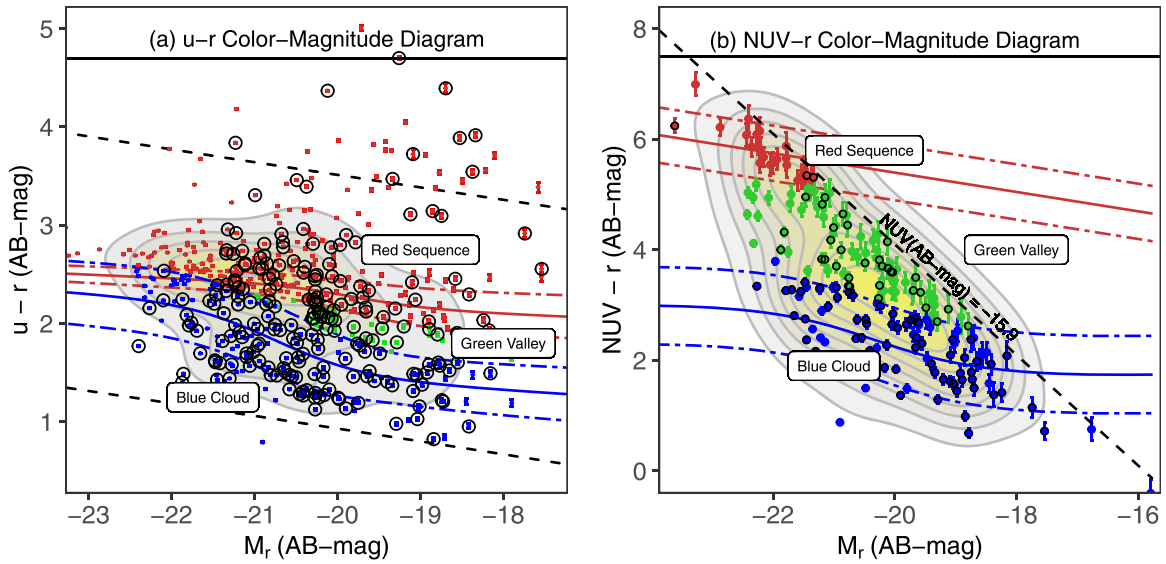

Figure 8. (a) The *u–r* color–magnitude relation and (b) the NUV–*r* color–magnitude relation in A1882. The black dashed lines represent the 95% prediction interval (PI) for all of the galaxies in the sample set. The red and blue lines represent the best fits for the RS and the BC. The gray dots represent the galaxies in A1882 in the color–color diagram. The black circles are the H_α emitters. The gray dashed line in panel (b) shows the NUV magnitude limit (= −15.9) for A1882.

low-level SFs are undetected in the optical color. Only ∼0.6% of the NUV blue galaxies are high-mass galaxies (log $M/M_\odot > 10.5$). This indicates that most of the massive galaxies have already moved to the RS in the past gigayear, although there are also a significant number of high-mass NUV GV galaxies, indicating low-level SF in the massive galaxies in the past gigayear.

In the intermediate-mass range, there is a larger fraction of blue galaxies in both the optical and UV colors. In addition, a large number of green intermediate-mass galaxies have been revealed. About one-fifth of the high-mass galaxies and intermediate-mass galaxies detected in the NUV are GV galaxies, and hence have undergone a change in their star-forming pattern (i.e., low-level SF episodes) in the past gigayear. The *u–r* color does not reflect these recent low-level SF episodes in the massive galaxies.

The dwarf galaxies have significantly more optically blue than red galaxies. The fractional numbers of the dwarf galaxies in NUV–*r* color are affected by the GALEX flux threshold, which severely undercounts the red and green dwarf galaxies.

4.3. The Spatial Distribution of Star-forming, Passive, and Transitioning Galaxies

Figures 11(a)–(d) show the optical and NUV color evolutions of galaxies as functions of the underlying large-scale structures (top panels), and the regions defined in Section 4.1 (see also Table 4) and Table 5 (bottom panels). The fractional number of the optically red galaxies is greater than that of the blue galaxies within the galaxy groups (∼60% of the galaxies in the galaxy groups are optically red), and comparable with the "swept-up" region (Figure 11(a)). The fractional number of the optically blue galaxies is the maximum within the galaxy population categorized as "others" (∼75%), i.e., the galaxies that do not lie within the groups, filaments, or the "swept-up" region.

The ratio of NUV red galaxies to blue galaxies is comparable within the groups, despite the absence of low-mass red galaxies, which are severely undercounted (Figure 11(b)). The fractional number of NUV massive red galaxies appears to fall sharply outside the groups that tend to harbor the massive red galaxies. About 56% of these NUV massive red galaxies, as detected by GALEX, are within the galaxy groups (i.e., Region 1), and ∼26% are in Region 3. However, the number of NUV blue galaxies shows a sharp decline from the galaxy population categorized as "others" to the galaxy population within the groups, filaments, and the "swept-up" region. This strongly indicates that the underlying large-scale structures have a role to play in the quenching of SF in the galaxies.

Figures 11(c)–(d) trace the optical and UV colors as functions of their radial distances from the assumed center of A1882. At a projected radial distance of $M/M_\odot R > 1.4 Mpc$ from the assumed center of A1882 (i.e., outside the groups and the "swept-up" region), the population is dominated by optically blue galaxies (Figure 11(c)). The fractional number of the optically red galaxies has the highest value in the group environment, indicating an overall decrease in the SF within the galaxy group environment over the past 2–3 Gyr. However, instead of progressively increasing outward from the group environment, the fractional number of the blue galaxies peaks in Region 4 (∼90% of the galaxies). Region 4 has a lower Σ (∼7 galaxies Mpc^{-2}) than both Region 3 (∼29 galaxies Mpc^{-2}) and Region 5 (∼17 galaxies Mpc^{-2}).

The fractional numbers of NUV blue galaxies in Region 1, Region 2, and Region 3 are comparable. However, similar to the optical counterpart, the fractional number of NUV blue galaxies drastically increases in Region 4, which has a much lower Σ than Region 3 and Region 5. This indicates that the lower Σ facilitates greater SF in the galaxies, and that the color–density relation is already in place at the very early stages of cluster formation.

Interestingly, the fractional numbers of NUV red and NUV blue galaxies are comparable in Region 5, which has a higher Σ than Region 4, and the fraction of the red galaxies also appears to be comparable to that in Region 1 (i.e., the groups).

The above results indicate that the galaxy color is tied very strongly to the local galaxy density, even in a complex structure like A1882. We identify the projected radial distance from the assumed center as a second-order evolutionary driver.

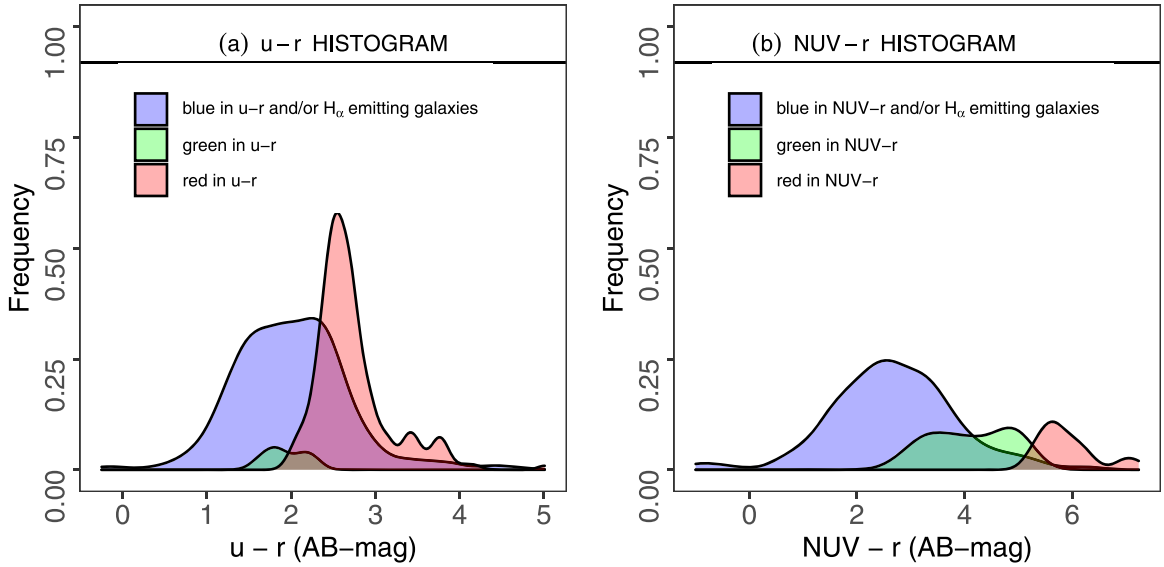

Figure 9. Histograms for the red, blue, and green galaxies, shown in red, blue, and green colors, respectively, in (a) u–r and (b) NUV–r colors. The RS, BC, and GV galaxies are represented by red, blue, and green colors, respectively, using the new classification based on the optical and UV colors, as well as H_α emissions.

4.4. The Spatial Locations of the Green Valley Galaxies in the NUV

The fractional number of NUV green galaxies increases inward from Region 5, and peaks in the "swept-up" region (i.e., Region 2), indicating intermediate- to high-mass galaxies undergoing low-level SF in the "swept-up" region, i.e., in the immediate infall region of the groups, in the past gigayear (Figures 11(b), (d)). This population is conspicuous by its absence from the "others."

Figure 12 shows the locations of the GV galaxies in the SuperGroup (the green filled circles), overlaid on a local galaxy density map. About 95% of these GV galaxies lie within $\mathcal{R} < 2.6$ Mpc from the assumed center of the SuperGroup, i.e., in Region 1, Region 2, and Region 3. About 27% of the NUV green galaxies lie within the galaxy groups (Region 1), and ∼68% of the NUV galaxies lie in the immediate infall region of A1882 (∼34% each in Region 2 and Region 3). It is interesting to note that although all of the three outer regions—Region 3, Region 4, and Region 5—have a large fraction of galaxies in the filaments (∼92%, ∼81%, and ∼53% of galaxies in the filaments, respectively), the majority of the NUV green galaxies that lie within the filaments (∼80%) are in Region 3 (a radial distance of $1.4 < \mathcal{R} < 2.6$ Mpc from the assumed center of A1882). Hence, most of the low-level SF in the galaxies is close to the infall region, where $\Sigma \geqslant 29$ galaxies Mpc^{-2}. Even though there are GV galaxies within the galaxy group environment, then, the transitioning of the galaxies takes place long before the galaxies are funneled into the galaxy groups.

Two distinct NUV green galaxy populations are shown in Figure 12:

1. *The optically blue galaxies that are green in the NUV*: the NUV green galaxies (shown in green) with blue dots indicate the galaxies that are optically blue. These galaxies were actively star-forming in the past 2–3 Gyr. However, they have only undergone low-level SF in the past 0.3–1 Gyr, as indicated by their NUV − r color. About 30% of the GV galaxies constitute this type of galaxy. Most of the galaxies in this population (∼84%) are in the immediate infall region of the groups (i.e., the "swept-up" region and the galaxies inside the filaments close to the group environment; $\mathcal{R} < 2.6$ Mpc), indicating preprocessing in the high-density infall region that suppressed the high-level SF, and led only to low-level SF, in the galaxies in the past 0.3–1 Gyr. If we look at the mass distribution of the optically blue, NUV green population, ∼46% are high-mass galaxies, and ∼54% are intermediate-mass galaxies.
2. *The optically red galaxies that are green in the NUV*: the NUV green galaxies (shown in green) with orange dots indicate the galaxies that are optically red. About 60% of the GV galaxies in the NUV are optically red. This galaxy population has been passive for 2–3 Gyr. However, the galaxies have undergone low-level SF in the past 0.3–1 Gyr, as indicated by the green NUV − r color. This suggests recent SF or the "rejuvenation" of the red galaxies (see Yi et al. 2005; Thomas et al. 2010) in at least the past gigayear. As discussed in Section 4.2, such rejuvenation can be caused by minor, gas-rich mergers in passive galaxies (Kaviraj et al. 2005), or the accretion of gas by RS galaxies from the intergalactic medium (Thilker et al. 2007).

All of the galaxies in this population are in the immediate infall region of the groups (i.e., the "swept-up" region and the galaxies inside the filaments close to the group environment; $\mathcal{R} < 2.6$ Mpc). All of the mass ranges show "rejuvenation" in the past 0.3–1 Gyr. About 69% of the intermediate-mass galaxies, 33% of the high-mass galaxies, and ∼33% of the dwarf galaxies in the NUV GV region are optically red.

Hence, about 20% of all of the high-mass galaxies and ∼7% of all of the intermediate-mass galaxies detected in the NUV, which were actively star-forming in the past 2–3 Gyr, are currently undergoing only low-level SF. None of the dwarf galaxies in our sample are in this population, possibly because they are undercounted in the NUV. On the other hand, about 10% of all of the high-mass galaxies and ∼20% of all of the intermediate-mass galaxies detected in the NUV, which were passive in the past 2–3 Gyr, are currently undergoing "rejuvenation."

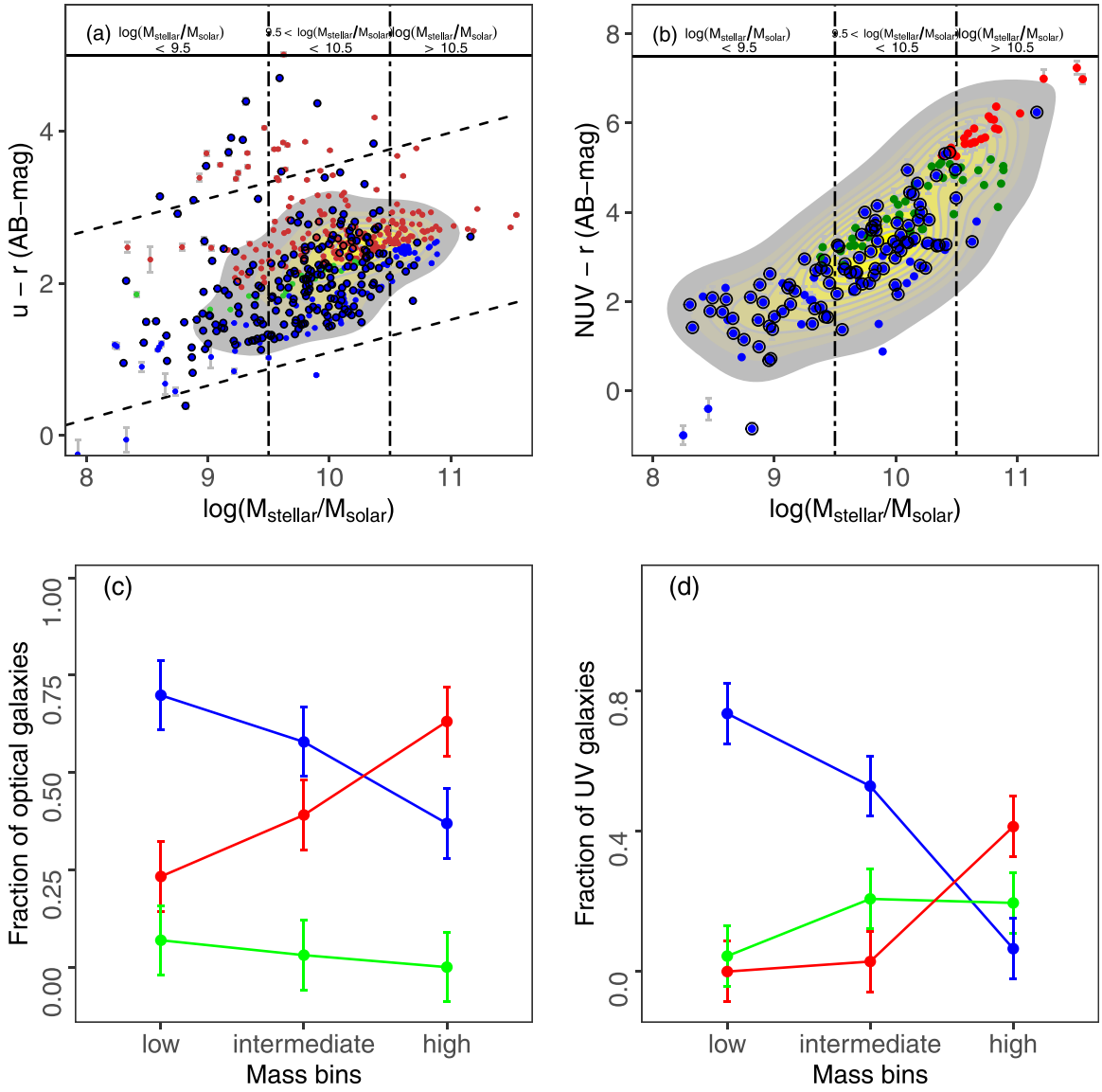

Figure 10. (a) *u–r* color–mass relation and (b) NUV–*r* color–mass relation in A1882. The red, blue, and green dots represent the RS, BC, and GV galaxies, respectively. The black open circles represent the H_α emitters, all of which have been reclassified as blue galaxies. The black dashed lines represent the 95% PI for all of the galaxies in the sample. (c) The fraction of optical galaxies and (d) the fraction of UV galaxies for different mass ranges. The galaxy mass bins are defined in Section 3.3. The RS, BC, and GV galaxies are represented by red, blue, and green colors, respectively, using the new classification based on the optical and UV colors, as well as H_α emissions.

We also detect five optically blue high-mass galaxies that are red in the NUV (marked by red stars), indicating quenching of these massive galaxies in the past 0.3–1 Gyr. However, the transformation of optically red galaxies to NUV blue galaxies (marked by blue stars) is only seen in the lower-mass galaxies ($\log M/M_\odot < 10$). This means that the rejuvenation in the massive galaxies in the past 0.3–1 Gyr is due to low-level SF, and not due to high-level continuous SF. These optically red, NUV blue galaxies are mostly within the galaxy groups or very close to them.

4.5. D_n*4000 Index,* H_α*, Optical Color, and UV Color Histograms for the Different Mass Bins*

The *D*4000 index or the 4000 Å break is the difference between the levels of continuum just blueward and redward of 4000 Å. In hot stars, multiply ionized elements reduce the opacity, and hence reduce the *D*4000 index. A strong *D*4000 index indicates a lack of hot, blue stars in the galaxy. Because of its smaller wavelength range, the *D*4000 index is less sensitive to the dust attenuation of the stars whose spectra cover these wavelengths, compared to the broadband color parameters (see Bruzual 1983; Hamilton 1985; Balogh et al. 1999; Kauffmann et al. 2003; Hathi et al. 2009; Haines et al. 2017).

The *D*4000 index is very sensitive to significant SF in the past 1 Gyr from the observed epoch, and also metallicity. A $D4000 \sim 1.5$ indicates an average age of 1 Gyr for the stellar population, and this value can be used to separate star-forming and quiescent galaxies (Kauffmann et al. 2003; Hathi et al. 2009; Haines et al. 2017).

We have used a narrow version of the *D*4000 index, i.e., the D_n4000 index as defined by Balogh et al. (1999). The D_n4000 index is much less sensitive to the reddening effect than the standard *D*4000.

The stellar population is assumed to have $D_n4000 \approx 1$ at birth, and to evolve redward (Balogh et al. 1999). In addition,

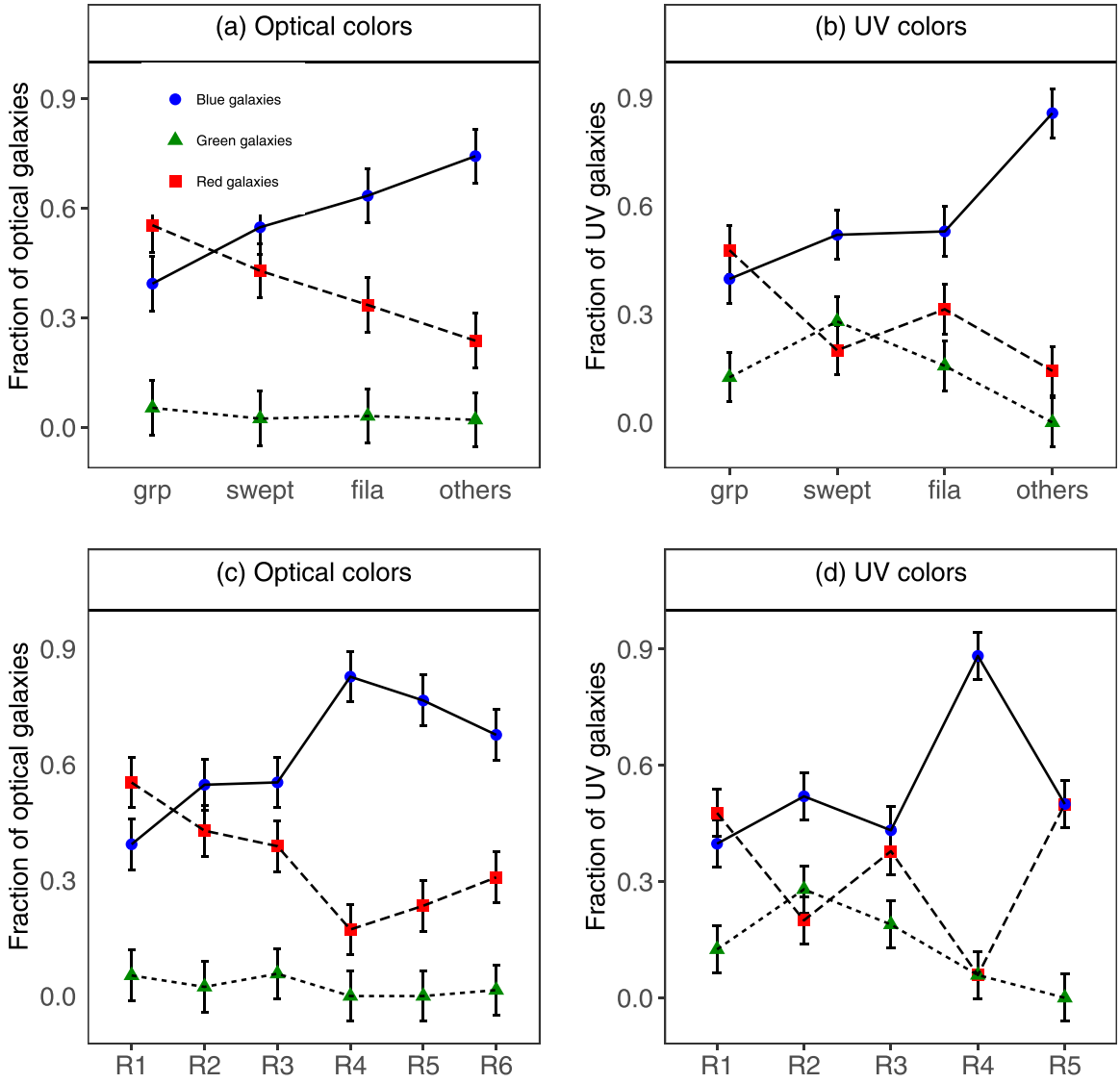

Figure 11. Fractional numbers of red, blue, and green galaxies in optical and UV colors as functions of their underlying structure, as described in Section 4.1 and Table 4 (top panels), and as functions of the regions described in Table 5 (bottom panels) in A1882. The fractional numbers of the optical and the NUV colors are shown in the left column and the right column, respectively. The RS, BC, and GV galaxies are represented by red, blue, and green colors, respectively, using the new classification based on the optical and UV colors, as well as H_α emissions.

the D_n4000 index has a well-defined upper limit of ∼2.3 for early-type galaxies. Hence, we have retained the D_n4000 index values only within the range $1 < D_n4000 < 2.3$ (Bruzual 1983; Hamilton 1985; Kauffmann et al. 2003; Kim et al. 2018).

Figures 13(a), (b) show the histograms of the u–r and NUV–r RS, GV, and BC galaxies in D_n4000 index bins. The modes of the overall population for each of the colors are shown by the black dashed and dotted lines. $D_n4000 \sim 1.5$ is shown by the black dotted line for reference.

In Figure 13(b), the modes of D_n4000 are well separated for the red and blue galaxies in NUV–r color, as expected. We find that the modes of the blue galaxies (shown by the blue histogram) and the red galaxies (shown by the red histogram) for both the u–r and NUV–r colors are $D_n4000 \sim 1.29$ and $D_n4000 \sim 1.86$, respectively. This is very similar to the values obtained by Kauffmann et al. (2003), who identified the peaks at ∼1.27 and ∼1.85, respectively. The NUV blue galaxies represent a younger stellar population, whereas the red galaxies, which peak at $D_n4000 > 1.86$, represent an older, metal-rich, mostly quiescent stellar population. A second, smaller peak in the NUV–r red galaxies points at the possibility of two distinct quiescent stellar populations, where the smaller peak has a smaller mean stellar age. However, all of the red galaxies have $D_n4000 > 1.5$. This means that all of the NUV red galaxies stopped forming stars at least 1 Gyr before the observed epoch.

The NUV–r GV galaxies peak at $D_n4000 > 1.5$. It is important to note that the photometric colors are obtained from the integrated light of the entire galaxy, whereas the spectral data are obtained only from the central regions of the galaxies. Hence, the NUV–r and u–r colors may not represent the same environments as the regions within the galaxies represented by D_n4000. The D_n4000 obtained from SDSS gives us the stellar age over a 3″ diameter, whereas the NUV data obtained from GALEX refer to a region even larger than the 5″ position-matching tolerance. It is likely that the low-level SF detected in the NUV GV galaxies is occurring in the outer regions of these galaxies, beyond the 3″ diameter. This result is

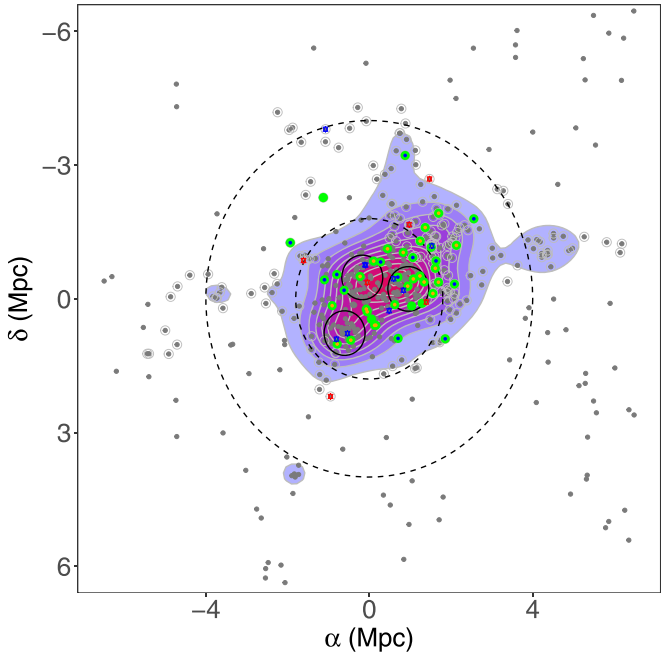

Figure 12. Local galaxy density map of A1882 overlaid with the GV galaxies in the NUV (in green), with red highlighting the densest regions. The green galaxies with blue and orange dots indicate the galaxies that are optically blue and red, respectively. The plus signs in black indicate H_α-emitting galaxies. The gray dots indicate all of the galaxies in A1882. The gray circles indicate the galaxies within the filaments.

similar to the evidence of low-level outer disk star formation in the GALEX Nearby Galaxies Survey (Gil de Paz et al. 2007; see also Thilker et al. 2007).

In Figure 13(a), almost all of the optically red galaxy population in the u–r color has $D_n4000 > 1.5$, as expected. The optically blue galaxy population in the u–r color has a significant number of galaxies with $D_n4000 > 1.5$. This population of u–r blue galaxies was star-forming in the past 2–3 Gyr from the observed epoch, but has been quiescent in the past 1 Gyr from the observed epoch, and contains mostly older, metal-rich galaxies.

Figure 14 shows the histogram of the D_n4000 index in mass bins. The peak values of D_n4000 are well separated for the high-mass galaxies (shown in brown) and the dwarf galaxies (shown in cyan). This signifies that the dwarf galaxies mostly consist of younger stellar populations, whereas the massive galaxies are older and metal-rich galaxies, which stopped forming stars at least 1 Gyr before the observed epoch. The intermediate-mass galaxies (shown in magenta) have comparable numbers of younger and older stellar populations. This is complemented by Figure 15, which shows that the dwarf galaxies have a higher fraction of H_α emitters (65%), and the high-mass galaxies are primarily non-H_α emitters (90%). The intermediate-mass galaxies have comparable numbers of H_α emitters and non-H_α emitters, where the H_α emitters are currently forming stars. Hence, a separation of the galaxy population into mostly star-forming, dwarf galaxies (log $M_\odot \leqslant 9.5$), on the one hand, and quiescent, high-mass galaxies (log $M_\odot \leqslant 10.5$), on the other hand, has been in place in A1882 for at least the past 1 Gyr.

4.6. Mass-dependent Evolutions of u–r and NUV–r Colors in Different Environments within A1882

In Figures 16(a)–(d), we trace the optical and UV color evolutions of the galaxies within the various underlying large-scale structures of A1882 (top panels), and within the different regions of A1882, as defined in Section 4.1 and Table 5 (middle panels), for the different mass bins. The mass bins are defined in Section 3.3. The color evolutions are traced for all galaxies (in black solid lines), as well as for three separate galaxy mass bins: high-mass galaxies (in the large brown solid circles), intermediate-mass galaxies (in the smaller solid magenta circles), and dwarf galaxies (in the smallest solid blue circles). Figures 16(a) and (c) show the overall reddening of the galaxies within the groups and the "swept-up" region in optical colors.

This indicates an overall suppression of SF in the past ∼2–3 Gyr. Figure 16(b) shows no such trend in NUV–r color within the different underlying large-scale structures, although Figure 16(d) shows a slight reddening of the NUV–r color in Region 1, Region 2, and Region 3, as compared to Region 4, highlighting the effect of radial distance and Σ in the quenching of SF in the galaxies. It is important to note that the majority of the galaxies in both the optical and UV colors are intermediate-mass galaxies (62% of the galaxies in the optical colors, and 56% of the galaxies in the NUV). Hence, the mean color for all of the galaxies in each bin is driven by the mean color of the intermediate-mass galaxies in that bin.

The color evolutions of the galaxies in the optical and UV are more pronounced if we trace them in separate mass bins. The optical color samples the red, dwarf galaxies much more effectively than the NUV color. Optically, the color evolution of the dwarf galaxies (log $M/M_\odot < 9.5$) is much more significant than that of the higher-mass galaxies. The mean u–r and NUV–r color for the high-mass galaxies are the reddest, whereas those of the dwarf galaxies are the bluest, at all radial distances from the core, and for all of the underlying large-scale structures. The colors of the galaxies in the individual mass bins are more separate in NUV–r color compared to u–r color.

Figure 16(c) shows a drastic reddening of the dwarf galaxies in the optical color as they approach the "swept-up" region. This indicates the quenching of dwarf galaxies in the "swept-up" region, i.e., in the immediate infall region of the group environment, in the past 2–3 Gyr. No such trend for the dwarf galaxies in observed in the NUV–r color, due to the GALEX flux threshold for low-luminosity galaxies, which severely cuts the red and green dwarf galaxies in NUV–r color.

The intermediate-mass galaxies within the groups, the "swept-up" region, and the filaments are significantly redder in NUV–r color compared to the galaxies categorized as "others" (Figure 16(b)). Figure 16(d) also shows a reddening of the intermediate-mass galaxies in Region 3 in NUV–r color, indicating a decrease in SF in the intermediate-mass galaxies at $\mathcal{R} < 2.6$ Mpc.

Figures 16(e)–(f) show the smoothed histograms of u–r color and NUV–r color, respectively, in the black dashed lines. The NUV–r color histograms of the high-mass, intermediate-mass, and the dwarf galaxies are shown in dark gray, yellow, and light gray colors, respectively. There is a clear bimodality in the optical and UV colors in the histograms for massive and dwarf galaxies. The NUV–r color histogram for the intermediate-mass galaxies peaks redward of the histogram for the dwarf galaxies, and blueward of that for the high-mass galaxies. Compared to the UV color, the optical color–magnitude diagram in A1882 does not show well-separated RS and BC, especially at the higher-mass end.

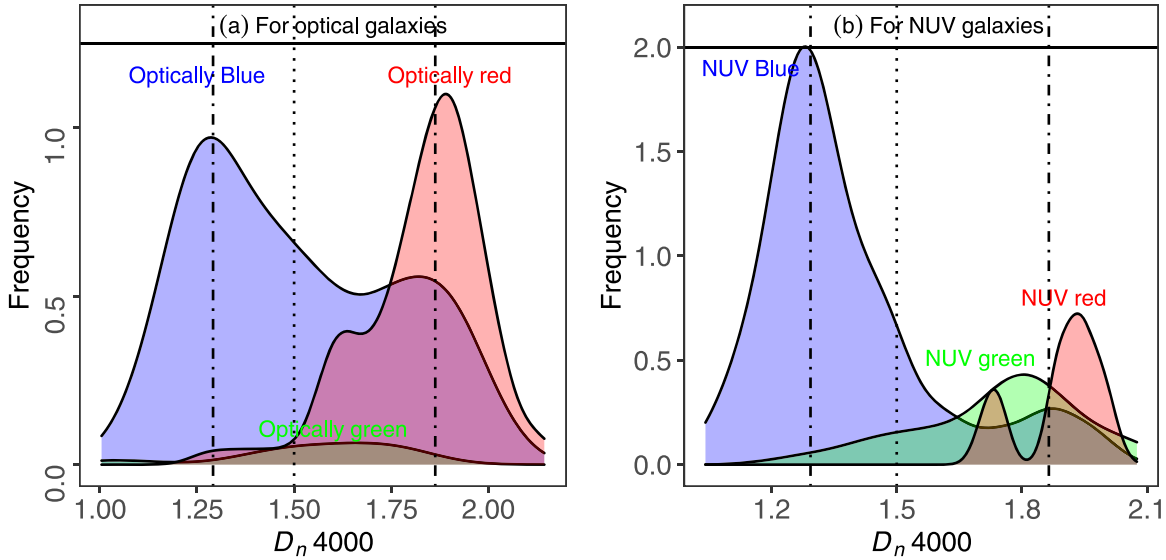

Figure 13. Smoothed histograms of the D_n4000 index for the red (shown in red), blue (shown in blue), and green galaxies (shown in green), in (a) optical colors and (b) NUV colors. The black dashed and dotted lines represent the modes of the entire population for each category. The black dotted line represents the D_n4000 index ∼1.5, which corresponds to a stellar population of 1 Gyr. The RS, BC, and GV galaxies are represented by the red, blue, and green colors, respectively, using the new classification based on the optical and UV colors, as well as H_α emissions.

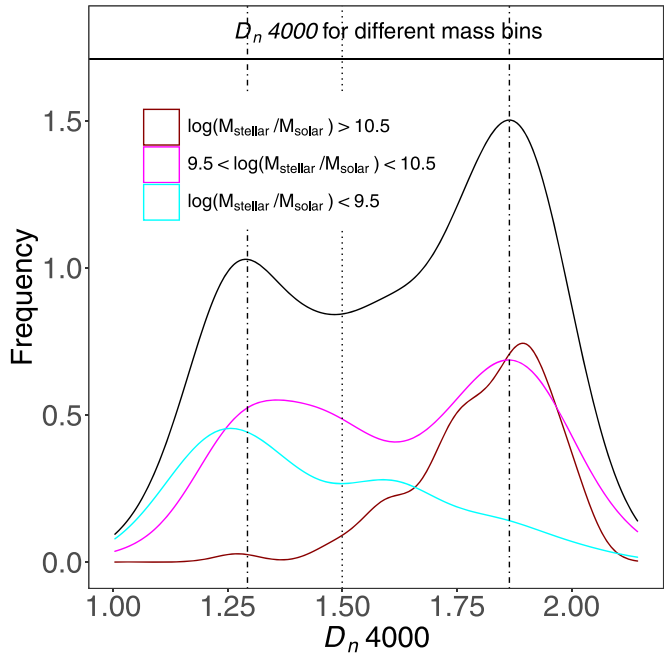

Figure 14. Smoothed histograms of the D_n4000 index for different mass bins. The black histogram represents all of the galaxies. The black dashed and dotted lines represent the modes of the entire population in each category. The black dotted line represents the D_n4000 index ∼1.5, which corresponds to a stellar population of 1 Gyr. The galaxy mass bins are defined in Section 3.3.

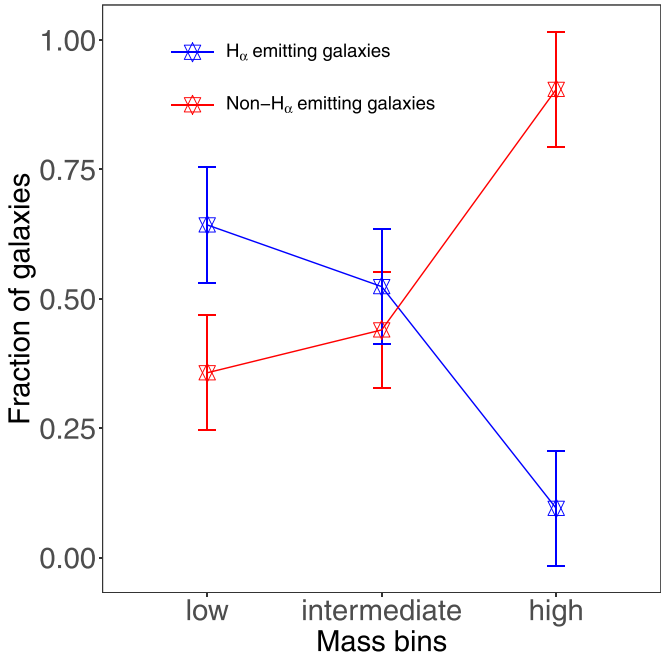

Figure 15. Fractions of H_α-emitting (in blue) and non-H_α-emitting galaxies (in blue) for different mass ranges. The galaxy mass bins are defined in Section 3.3.

5. Results and Discussion

We have amassed the largest optical catalog for A1882, with 526 member galaxies, using the MMT and Hectospec, the GAMA survey, the SDSS archive, NED, and the Gemini Multi-Object Spectrographs. We have complemented the optical catalog with the GALEX data, which includes 191 NUV detections. We have identified at least three primary feeding filaments in the cluster outskirts of A1882, which accrete the galaxies asymmetrically mostly along the direction of the R.A., through which most of the galaxies are eventually funneled into the groups. The local galaxy density Σ increases sharply near the three major groups of galaxies. However, we observe distinct overdensities at various R in the SuperGroup outskirts, indicating that A1882 is still in the process of growth and accretion. The infall pattern of the member galaxies in the SuperGroup has a characteristic trumpet shape that is usually observed in more massive and relaxed clusters, like the Coma Cluster, even at this early stage of virialization.

The average velocity dispersion in A1882 is 620 km s^{-1}. This value is much lower than the velocity dispersion of massive and relaxed clusters, like the Coma cluster, which has a velocity dispersion of ∼1000 km s^{-1} (Struble & Rood 1999).

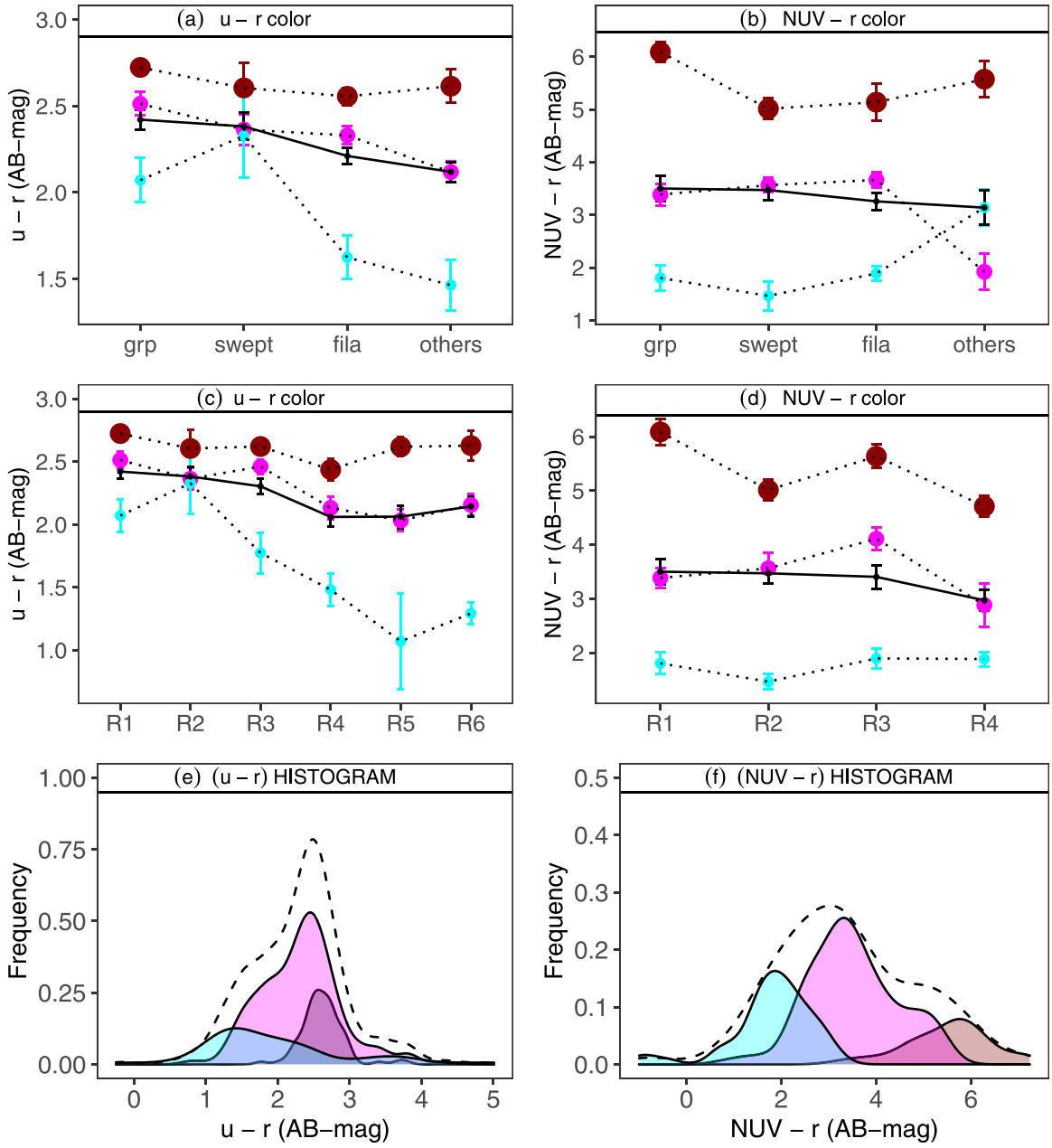

Figure 16. Top panels: the mean u–r color and NUV–r color, respectively, with standard error bars, for galaxies of all masses (in black), the high-mass galaxies (the large brown solid circles), the intermediate-mass galaxies (the smaller solid magenta circles), and the dwarf galaxies (the smallest solid blue circles) within the various underlying large-scale structures of A1882. The galaxy mass ranges are as defined in Section 3.3. Middle panels: the evolutions of the mean u–r color and NUV–r color with radial distance from the assumed core of A1882. Bottom panels: smoothed histograms of the color distributions in dwarf galaxies (cyan), intermediate-mass galaxies (magenta), and massive galaxies (brown). The dotted lines represent smoothed histograms of all of the galaxies for u–r color and NUV–r color, respectively. The RS, BC, and GV galaxies are represented by the red, blue, and green colors, respectively, using the new classification based on the optical and UV colors, as well as H_α emissions.

Filament 1 shows evidence of an undetected smaller galaxy group, or a galaxy group that is in the early stages of assembly. We have used optical and NUV colors to determine the evolution of the galaxies as they are funneled into the galaxy groups at the center of A1882. The overabundance of GV galaxies in NUV–r color indicates that the UV colors are much better diagnostics of ongoing low-level SF compared to their optical counterpart.

Here are the questions we set out to address in this paper:

1. At which point during the early evolutionary history of the formation of a cluster does one see significant galaxy transformations that lead to the overabundance of optically red galaxies that are observed at the core of the present-day clusters? In other words, are the well-established color–color and color–density relations seen in the present-day clusters also seen in an unrelaxed cluster like A1882?
2. Is there evidence of galaxy transformation as a function of both the number density of the galaxies and the spatial locations of the galaxies within the structure?
3. Is the galaxy transformation dependent on the mass of the galaxy?

Here is a summary of the main results that address the above questions:

1. We observe that A1882 has well-formed RS, GV, and BC populations in photometric colors, similar to more virialized clusters like Coma and Virgo. The higher-mass galaxies in A1882 peak at the redward side of the color scale, and they are more constrained in the u–r color, as compared to the dwarf galaxies. High-mass NUV blue stars are conspicuous by their absence, indicating that most of the massive galaxies ($\log M/M_{\odot} > 10.5$) have already moved to the NUV RS, and stopped forming stars in the past gigayear, even before they entered the far outskirts of A1882. Hence, evolutionary processes similar to those of more relaxed groups have already taken place in this unrelaxed cluster system. However, the RS in A1882 is not as tightly constrained as it is in more virialized clusters like Coma and Virgo, indicating a larger spread in the ages of the RS galaxies in A1882 compared to more well-formed clusters. The red galaxies in A1882 were more likely formed due to stochastic episodes arising from various environmental mechanisms, like mergers, ram pressure stripping, harassments, etc., spread over different epochs. The intrinsic scatter within the RS will likely reduce as the system evolves.
2. We also find that, similar to the previous results found for SuperGroup 1120–1202 (Gonzalez et al. 2005; Kautsch et al. 2008), there is already a higher fraction of RS galaxies (60% of optical RS and 50% of NUV RS) in the individual groups in SuperGroup A1882, compared to those in the far outskirts, indicating an overall decrease in the SF within the galaxy group environment at least in the past 2–3 Gyr. The immediate infall region, i.e., the "swept-up" region, also has a comparable fraction of red galaxies, indicating that the SF in the galaxies has been suppressed even before the galaxies enter the galaxy group environment. The overall decrease in the fraction of blue galaxies and the increase in the fraction of red galaxies within the groups, filaments, and the "swept-up" region indicate more preprocessing in the galaxies within the large-scale structures (the groups and filaments) and in the immediate infall region of the galaxies (the "swept-up" region) compared to the galaxy population in the "others," which contains a higher fraction of blue galaxies in both the optical and UV colors.

   In the context of the projected radial distance from the assumed center of A1882, we find that at a projected radial distance of $\mathcal{R} > 1.4$ Mpc from the assumed center of A1882 (i.e., outside the groups and the "swept-up" region), the population is dominated by optically blue galaxies.

   However, Region 4, which is at a closer projected radial distance from the central group environment than Region 5, but has a much lower Σ than Region 5, contains a higher fraction of optically blue galaxies and a lower fraction of optically red galaxies. This indicates increased SF in the low-density Region 4, as compared to Region 5, even though it is closer to the group environment. We identify Σ as the primary driver, and the projected radial distance from the assumed center as a second-order evolutionary driver.

   Hence, similar to the findings of the past three decades for galaxy evolutions in cluster environments, our results show that Σ, the proximity to the central gravitational potential $\mathcal{R}$, as well as the underlying large-scale structure are important driving mechanisms for galaxy transformation, even within a complex, unvirialized cluster environment like A1882.

   We also constrain how the galaxy transformation is dependent on the mass of the galaxy.
3. We show that the dwarf galaxies ($\log M_{\odot} \leqslant 9.5$) are mostly star-forming, and that the high-mass galaxies ($\log M_{\odot} \leqslant 10.5$) are quiescent and metal-rich. The optical color evolution of the dwarf galaxies is much more pronounced than that of the higher-mass galaxies. We see the quenching of dwarf galaxies in the "swept-up" region ($\mathcal{R} < 1.4$ Mpc), i.e., in the immediate infall region of the group environment, in the past 2–3 Gyr. The high-mass galaxies appear to have undergone most of the transformations, and are already on the RS before they encounter the A1882 environment. However, the massive galaxies are not all 'red and dead'. A significant number of these galaxies show transformation due to low-level SF ("rejuvenation"). Most of these transformations occur in the immediate infall region of the group environment ($\mathcal{R} < 2.6$ Mpc). The intermediate-mass galaxies also show an overall reddening at distances $\mathcal{R} < 2.6$ Mpc from the assumed center of A1882. Further, it is likely that the low-level SF detected in the NUV GV galaxies is primarily occurring in the outer regions of these galaxies, beyond the 3″ diameter, which is not sampled by D_n4000.

To summarize, the optical color evolution (over the past 2–3 Gyr) of the dwarf galaxies is most evident at roughly twice the virial radius of the groups, whereas the high- and intermediate-mass GV galaxies indicate that the recent transformations in the past gigayear occur within roughly four times the virial radius. Hence, the filaments and the immediate infall region play a significant role in the suppression of SF in the galaxies even before they enter the group environment.

We conclude that the physical mechanisms that suppress SF, primarily in the intermediate-mass and dwarf galaxies, must be those that take effect in environments that have lower densities than the galaxy groups, and hence occur even before the galaxies fall into the high-density, high-velocity dispersion fields of the galaxy groups. This is similar to the findings of Saintonge et al. (2008) and Tran et al. (2009), who found evidence for the quenching of SF in galaxies even before they enter the group environment. This strongly indicates low density-driven galaxy transformation mechanisms.

In hierarchical mergers of galaxies, galaxy mergers can cause the combined dark matter halo to cross a critical halo mass ($>10^{12} M_{\odot}$), generating a shock in the accreting gas, as well as gas heating, thereby preventing it from cooling and forming stars, rendering them red and dead by redshift $z \sim 0$. If the galaxies reside in smaller halos, the gas may not be shock-heated. This allows for SF and the subsequent regulation of the same by several feedback mechanisms. This model is favored by the hierarchical structure formation theory in the ΛCDM model. Combined with the fact that these massive galaxies form a tight and narrow red sequence, and are possibly primarily massive ellipticals, it strongly implies dry mergers as the driving force causing the observed color of these galaxies. Dry mergers occur between already gas-poor, passive galaxies. Hence, it does not lead to significant changes in the SF in these galaxies. This also explains why the color evolution of the massive galaxies is not as drastic as it is in the lower-mass galaxies. However, at least 30% of these massive galaxies show

signs of rejuvenation close to the group environment. This indicates that at least some of these massive galaxies are undergoing low-level SF.

Dwarf galaxies and intermediate-mass galaxies undergo significant transformation long before they enter the galaxy group environment. The filaments and the immediate infall region play a significant role in suppressing the SF in these galaxies. We propose galaxy–galaxy wet mergers, which work in the low-density and low-velocity dispersion cases. We conclude that wet mergers may cause more drastic changes to the star-forming capabilities of dwarf galaxies, which are primarily emission line galaxies, compared to the intermediate-mass galaxies. This may lead to a more drastic color evolution and a lower D_n4000 index evolution in the dwarf galaxies compared to higher-mass galaxies.

6. Summary and Conclusions

Since unrelaxed clusters at high redshifts are hard to detect, and are rare at lower redshifts, we have little understanding of the galaxy transformations occurring in these environments. However, the galaxy bimodality that we see in the present-day clusters traces back to the evolutionary mechanisms in the earlier phases of cluster formation. This makes these unrelaxed cluster environments an inevitable part of the narrative in the study of galaxy evolution, in addition to telling us what happened in the past evolutionary history of a rich cluster, like Coma. Our results for the intermediate-mass and dwarf galaxies are in agreement with those for the SuperGroups Eridanus and SG1120-1202, which show an overabundance of early-type galaxies, indicating that morphological preprocessing similar to that occurring in rich clusters has already taken place in these early systems, and possibly within the filaments (Gonzalez et al. 2005; Kautsch et al. 2008; Fadda et al. 2013). We also find that the evolution of optical and NUV colors is not only dependent on the Σ and proximity to the central gravitational potential, but also on the galaxy mass (McKinley et al. 2018).

Portions of this work were presented by A.S. to the University of Alabama in partial fulfillment of the requirements for the Ph.D.

The observations reported here were obtained at the MMT Observatory, a joint facility of the University of Arizona and the Smithsonian Institution. We thank the MMT staff for their very skillful help in making the MMT and Hectospec observations.

Funding for SDSS and SDSS-II has been provided by the Alfred P. Sloan Foundation, the Participating Institutions, the National Science Foundation, the U.S. Department of Energy, the National Aeronautics and Space Administration, the Japanese Monbukagakusho, the Max Planck Society, and the Higher Education Funding Council for England. The SDSS website is http://www.sdss.org/.

The SDSS is managed by the Astrophysical Research Consortium for the Participating Institutions. The Participating Institutions are the American Museum of Natural History, Astrophysical Institute Potsdam, University of Basel, University of Cambridge, Case Western Reserve University, University of Chicago, Drexel University, Fermilab, the Institute for Advanced Study, the Japan Participation Group, Johns Hopkins University, the Joint Institute for Nuclear Astrophysics, the Kavli Institute for Particle Astrophysics and Cosmology, the Korean Scientist Group, the Chinese Academy of Sciences (LAMOST), Los Alamos National Laboratory, the Max Planck Institute for Astronomy, the Max Planck Institute for Astrophysics, New Mexico State University, Ohio State University, University of Pittsburgh, University of Portsmouth, Princeton University, the United States Naval Observatory, and the University of Washington. GAMA is a joint European-Australasian project based around a spectroscopic campaign using the Anglo-Australian Telescope. The GAMA input catalog is based on data taken from the SDSS and the UKIRT Infrared Deep Sky Survey. Complementary imaging of the GAMA regions is being obtained by a number of independent survey programs, including GALEX Medium Imaging Surveys (MIS), VLT Survey Telescope Kilo-Degree Survey (VST KiDS), VISTA Kilo-Degree Infrared Galaxy Survey (VIKING), Wide-field Infrared Survey Explorer (WISE) Herschel-Asteroid Terrestrial-impact Last Alert System (ATLAS), Giant Metrewave Radio Telescope (GMRT), and Australian Square Kilometre Array Pathfinder (ASKAP), providing UV-to-radio coverage. GAMA is funded by the Science and Technology Facilities Council (STFC) (UK), the Australian Research Council (ARC) (Australia), the Australian Astronomical Optics (AAO), and the participating institutions. The GAMA website is http://www.gama-survey.org/.

We acknowledge the support from NASA James Webb Space Telescope (JWST) Interdisciplinary Scientist grants NAG5−12460, NNX14AN10G, and 80NSSC18K0200 from Goddard Space Flight Center (GSFC).

ORCID iDs

Aparajita Sengupta https://orcid.org/0000-0003-3490-4203
William C. Keel https://orcid.org/0000-0002-6131-9539
Glenn Morrison https://orcid.org/0000-0003-2310-4497
Rogier A. Windhorst https://orcid.org/0000-0001-8156-6281
Neal Miller https://orcid.org/0000-0003-1076-7558
Brent Smith https://orcid.org/0000-0002-0648-1699

References

Alam, S., & Albareti, F. D. 2015, ApJS, 219, 12
Baldry, I. K., Balogh, M. L., Bower, R. G., et al. 2006, MNRAS, 373, 469
Baldry, I. K., Glazebrook, K., Brinkmann, J., et al. 2004, ApJ, 600, 681
Balogh, M. L., Baldry, I. K., Nichol, R., et al. 2004, ApJL, 615, L101
Balogh, M. L., Morris, S. L., Yee, H. K. C., Carlberg, R. G., & Ellingson, E. 1999, ApJ, 527, 54
Bell, E. F., & de Jong, R. S. 2001, ApJ, 550, 212
Berrier, J. C., Stewart, K. R., Bullock, J. S., et al. 2009, ApJ, 690, 1292
Blanton, M. R., Dalcanton, J., Eisenstein, D., et al. 2001, AJ, 121, 2358
Blanton, M. R., Hogg, D. W., Bahcall, N. A., et al. 2003, ApJ, 594, 186
Brough, S., Forbes, D. A., Kilborn, V. A., & Couch, W. 2006, MNRAS, 370, 1223
Bruzual A., G. 1983, ApJ, 273, 105
Cardelli, J. A., Clayton, G. C., & Mathis, J. S. 1989, ApJ, 345, 245
Colless, M., Dalton, G., Maddox, S., et al. 2001, MNRAS, 328, 1039
Cooper, M. C., Newman, J. A., Coil, A. L., et al. 2007, MNRAS, 376, 1445
Dressler, A. 1980, ApJ, 236, 351
Dressler, A., Oemler, A., Jr., Couch, W. J., et al. 1997, ApJ, 490, 577
Dressler, A., Smail, I., Poggianti, B. M., Butcher, H., Couch, W. J., Ellis, R. S., & Oemler, A., Jr. 1999, ApJ, 122, 51
Einasto, Maret, Deshev, Boris, Tenjes, Peeter, et al. 2020, A&A, 641, A172
Erkurt, A., Tektunali, H. G., Hudaverdi, M., & Ercan, E. N. 2009, POBeo, 86, 305
Evans, J. D. 1996, Straightforward Statistics for the Behavioral Sciences (Pacific Grove, CA: Brooks/Cole Publishing)
Fabricant, D., Fata, R., Roll, J., et al. 2005, PASP, 117, 1411
Fabricant, D. G., Kurtz, M. J., Geller, M. J., et al. 2008, PASP, 120, 1222

Fadda, D., Biviano, A., Durret, F., & Edwards, L. O. 2013, AAS Meeting, 231, 243.07
Fassbender, R., Nastasi, A., Böhringer, H., et al. 2011, A&A, 527, L10
Fujita, Y. 2004, PASJ, 56, 29
Gil de Paz, A., Boissier, S., Madore, B. F., et al. 2007, ApJS, 173, 185
Gomez, P. L., Miller, C. J., Ingraham, P. J., & Sifon, C. 2010, BAAS, 42, 533
Gómez, P. L., Nichol, R. C., Miller, C. J., et al. 2003, ApJ, 584, 210
Gonzalez, A. H., Tran, K.-V. H., Conbere, M. N., & Zaritsky, D. 2005, ApJL, 624, L73
Haines, C. P., Iovino, A., Krywult, J., et al. 2017, A&A, 605, A4
Hamilton, D. 1985, ApJ, 297, 371
Hashimoto, Y., Oemler, A., Jr., Lin, H., & Tucker, D. L. 1998, ApJ, 499, 589
Hathi, N. P., Ferreras, I., Pasquali, A., et al. 2009, ApJ, 690, 1866
Huchra, J. P., & Geller, M. J. 1982, ApJ, 257, 423
Kauffmann, G., Heckman, T. M., White, S. D. M., et al. 2003, MNRAS, 341, 54
Kauffmann, G., White, S. D. M., Heckman, T. M., et al. 2004, MNRAS, 353, 713
Kautsch, S. J., Gonzalez, A. H., Soto, C. A., et al. 2008, ApJL, 688, L5
Kaviraj, S., Devriendt, J. E. G., Ferreras, I., & Yi, S. K. 2005, MNRAS, 360, 60
Kaviraj, S., Schawinski, K., et al. 2007, ApJS, 173, 619
Kennicutt, R. C., Jr. 2004, yCat, 7141
Kim, K., Malhotra, S., Rhoads, J. E., et al. 2018, ApJ, 867, 118
Lewis, I., Balogh, M., De Propris, R., et al. 2002, MNRAS, 334, 673
Liske, J., & Baldry, I. K. 2015, MNRAS, 452, 2087
Mahajan, S., Haines, C. P., & Raychaudhury, S. 2010, MNRAS, 404, 1745
Mahajan, S., Haines, C. P., & Raychaudhury, S. 2011, MNRAS, 412, 1098
Martin, D. C., Fanson, J., et al. 2005, ApJL, 619, L1
Martin, D. C., Wyder, T. K., & Schiminovich, D. 2007, ApJS, 173, 342
McGee, S. L., Balogh, M. L., Bower, R. G., Font, A. S., & McCarthy, I. G. 2009, MNRAS, 400, 937
McKinley, B., Tingay, S. J., Carretti, E., et al. 2018, MNRAS, 474, 4056
Miller, C. J., Gomez, P. L., Sifon, C. A., et al. 2010, BAAS, 41, 829
Morrison, G. E., Owen, F. N., Ledlow, M. J., et al. 2003, ApJS, 146, 267
Morrissey, P., Conrow, T., Barlow, T. A., et al. 2007, ApJS, 173, 682
Owers, M. S., Baldry, I. K., Bauer, A. E., et al. 2013, ApJ, 772, 104
Pimbblet, K. A., Smail, I., Kodama, T., et al. 2002, MNRAS, 331, 333
Planck Collaboration, Aghanim, N., Akrami, Y., et al. 2020, A&A, 641, A6
Poggianti, B. M., von der Linden, A., De Lucia, G., et al. 2006, ApJ, 642, 188
Postman, M., Franx, M., Cross, N. J. G., et al. 2005, ApJ, 623, 721
Postman, M., & Geller, M. J. 1984, ApJ, 281, 95
Rood, H. J. 1970, ApJ, 162, 333
Saintonge, A., Tran, K.-V. H., & Holden, B. P. 2008, ApJL, 685, L113
Salim, S. 2014, SerAJ, 189, 1
Salim, S., Rich, R. M., Charlot, S., et al. 2007, ApJS, 173, 267
Schawinski, K., Urry, C. M., Simmons, B. D., et al. 2014, MNRAS, 440, 889
Smail, I., Dressler, A., Couch, W. J., et al. 1997, ApJS, 110, 213
Smith, G. P., Treu, T., Ellis, R. S., Moran, S. M., & Dressler, A. 2005, ApJ, 620, 78
Spitzer, L., Jr., & Baade, W. 1951, ApJ, 113, 413
Springel, V., Frenk, C. S., & White, S. D. M. 2006, Natur, 440, 1137
Struble, M. F., & Rood, H. J. 1999, ApJS, 125, 35
Thilker, D. A., Boissier, S., Bianchi, L., et al. 2007, ApJS, 173, 572
Thomas, D., Maraston, C., Schawinski, K., Sarzi, M., & Silk, J. 2010, MNRAS, 404, 1775
Tran, K.-V. H., Saintonge, A., Moustakas, J., et al. 2009, ApJ, 705, 809
Treu, T., Ellis, R. S., Kneib, J. P., et al. 2003, ApJ, 591, 53
Vijayaraghavan, R., & Ricker, P. M. 2013, MNRAS, 435, 2713
Wyder, T. K., Martin, D. C., Schiminovich, D., et al. 2007, ApJS, 173, 293
Yi, S. K., Yoon, S.-J., Kaviraj, S., et al. 2005, ApJL, 619, L111
York, D. G., Adelman, J., Anderson, J. E., Jr., et al. 2000, AJ, 120, 1579